

Pages S1-S77

## Supporting Information

### **Probing electronic structure of $[\text{Ru}(\text{L}^1)_2]^z$ ( $z = 0, 1+$ and $2+$ ) ( $\text{H}_2\text{L}^1$ : a tridentate 2-aminophenol derivative) complexes in three ligand redox levels**

**Anannya Saha, Amit Rajput, Puneet Gupta and Rabindranath Mukherjee\***

---

## Figures

- Fig. S1** Positive-ion ESI-MS spectra of  $[\text{Ru}(\text{L}^1)_2]$  (**1**).
- Fig. S2**  $^1\text{H}$  NMR spectrum (400 MHz,  $\text{CDCl}_3$ ) of **1** at 298 K.
- Fig. S3** Positive-ion ESI-MS spectra of  $[\mathbf{1}^{\text{OX1}}](\text{PF}_6)\bullet\text{CH}_2\text{Cl}_2$ .
- Fig. S4** Positive-ion ESI-MS spectra of  $[\text{Ru}(\text{L}^1)_2](\text{BF}_4)_2\bullet\text{H}_2\text{O}$ .
- Fig. S5** Cyclic voltammogram (100 mV/s) of a 0.5 mM solution of  $[\mathbf{1}^{\text{OX1}}](\text{PF}_6)\bullet\text{CH}_2\text{Cl}_2$  in  $\text{CH}_2\text{Cl}_2$  (0.1 M in TBAP; 298 K) at a platinum working electrode.
- Fig. S6** Cyclic voltammogram (100 mV/s) of a 0.5 mM solution of **3** /  $[\mathbf{1}^{\text{OX2}}](\text{BF}_4)_2\bullet\text{H}_2\text{O}$  in  $\text{CH}_2\text{Cl}_2$  (0.1 M in TBAP; 298 K) at a platinum working electrode.
- Fig. S7**  $^1\text{H}$  NMR spectrum (400 MHz,  $\text{CDCl}_3$ ) of **3** /  $[\mathbf{1}^{\text{OX2}}](\text{BF}_4)_2\bullet\text{H}_2\text{O}$  at 298 K.
- Fig. S8** XPS of Ru 3d and C 1s core level for **1–3**.
- Fig. S9** XPS of N 1s core level for **1** and **3**.
- Fig. S10** X-band EPR spectra for solid  $[\mathbf{1}^{\text{OX1}}](\text{PF}_6)\bullet\text{CH}_2\text{Cl}_2$  at 150 K and at 298 K
- Fig. S11** X-band EPR spectrum of  $[\mathbf{1}^{\text{OX1}}]^{1+}$  in  $\text{CHCl}_3\text{-C}_6\text{H}_5\text{CH}_3$  (1:1, v/v) in the temperature range 120–318 K.
- Fig. S12** Modulation amplitude dependent X-band EPR Spectrum of  $[\mathbf{1}^{\text{OX1}}]^{1+}$  in  $\text{CHCl}_3\text{-C}_6\text{H}_5\text{CH}_3$  (1:1, v/v) at 120 K.
- Fig. S13** Mulliken spin population and qualitative MO diagram of the magnetic-orbitals of **1**, using BS-DFT calculation.
- Fig. S14** Computational model system used for DFT calculations (QRO analysis).
- Fig. S15** Qualitative frontier MO diagram for **1** ( $S = 1$ ) of QROs analysis.
- Fig. S16** Qualitative QRO diagram of  $[\mathbf{1}^{\text{OX1}}]^{1+}$  ( $S = 1/2$ , B3LYP-QRO).
- Fig. S17** Qualitative frontier MO diagram for  $[\mathbf{1}^{\text{OX1}}]^{1+}$  ( $S = 3/2$ , B3LYP-QRO).
- Fig. S18** Qualitative frontier MO diagram for  $[\mathbf{1}^{\text{OX2}}]^{2+}$  ( $S = 1$ , B3LYP-QRO).
- Fig. S19** Electronic spectra of **1**,  $[\mathbf{1}^{\text{OX1}}]^{1+}$ , and  $[\mathbf{1}^{\text{OX2}}]^{2+}$  in  $\text{CH}_2\text{Cl}_2$ .
- Fig. S20** TD-DFT-Calculated electronic spectra of **1**,  $[\mathbf{1}^{\text{OX1}}]^{1+}$ , and  $[\mathbf{1}^{\text{OX2}}]^{2+}$ , using B3LYP.
- Fig. S21** Representative molecular-orbitals involved in TD-DFT transitions of **1**, using CAM-B3LYP.
- Fig. S22** Representative molecular-orbitals involved in TD-DFT transitions of **1**, using B3LYP.

**Fig. S23** Representative MOs involved in TD-DFT transitions of  $[1^{OX1}]^{1+}$ , using CAM-B3LYP.

**Fig. S24** Representative MOs involved in TD-DFT transitions of  $[1^{OX1}]^{1+}$ , using B3LYP.

**Fig. S25** Representative MOs involved in TD-DFT transitions of  $[1^{OX2}]^{2+}$ , using CAM-B3LYP.

**Fig. S26** Representative MOs involved in TD-DFT transitions of  $[1^{OX2}]^{2+}$ , using B3LYP.

**Fig. S27** TD-DFT calculated spectra of free ligand in its  $(L^{ISQ})^{*-}$  redox level using CAM-B3LYP level of theory.

**Fig. S28** TD-DFT calculated spectra of free ligand in its  $(L^{IBQ})^0$  redox level using CAM-B3LYP level of theory.

## **Tables**

**Table S1** Crystal data and structure refinement parameters for **1** at 100 K and at 298 K

**Table S2** Crystal data and structure refinement parameters for **2** and **3** at 100 K and 298 K

**Table S3** Bond angles for **1**, **2** and **3**

**Table S4** Comparison of experimental bond lengths (X-ray) with calculated bond lengths (MOS values) (Å) of **1**, **2** and **3** at 298 K

**Table S5** DFT-optimized cartesian coordinates of **1**, using CAM-B3LYP-level of theory

**Table S6** DFT-optimized cartesian coordinates of  $[1^{OX1}]^{1+}$ , using CAM-B3LYP-level of theory

**Table S7** DFT-optimized cartesian coordinates of  $[1^{OX2}]^{2+}$ , using CAM-B3LYP-level of theory

**Table S8** X-ray determined and calculated (BS-DFT and DFT-QRO) bond lengths (Å) of **1**

**Table S9** X-ray determined and calculated (BS-DFT and DFT-QRO) bond lengths (Å) of  $[1^{OX1}]^{1+}/\mathbf{2}$

**Table S10** X-ray determined and calculated (BS-DFT and DFT-QRO) bond lengths (Å) of  $[1^{OX2}]^{2+}/\mathbf{3}$

**Table S11** Mulliken spin population for **1** and  $[1^{OX1}]^{1+}$ , using CAM-B3LYP and B3LYP

**Table S12** Computed energy values of CSS and BS solution for **1**, using CAM-B3LYP and B3LYP

**Table S13** Computed energy values for all three possible spin states for  $[1^{OX1}]^{1+}$ , using CAM-B3LYP

**Table S14** TD-DFT-calculated electronic transitions for **1**, using CAM-B3LYP

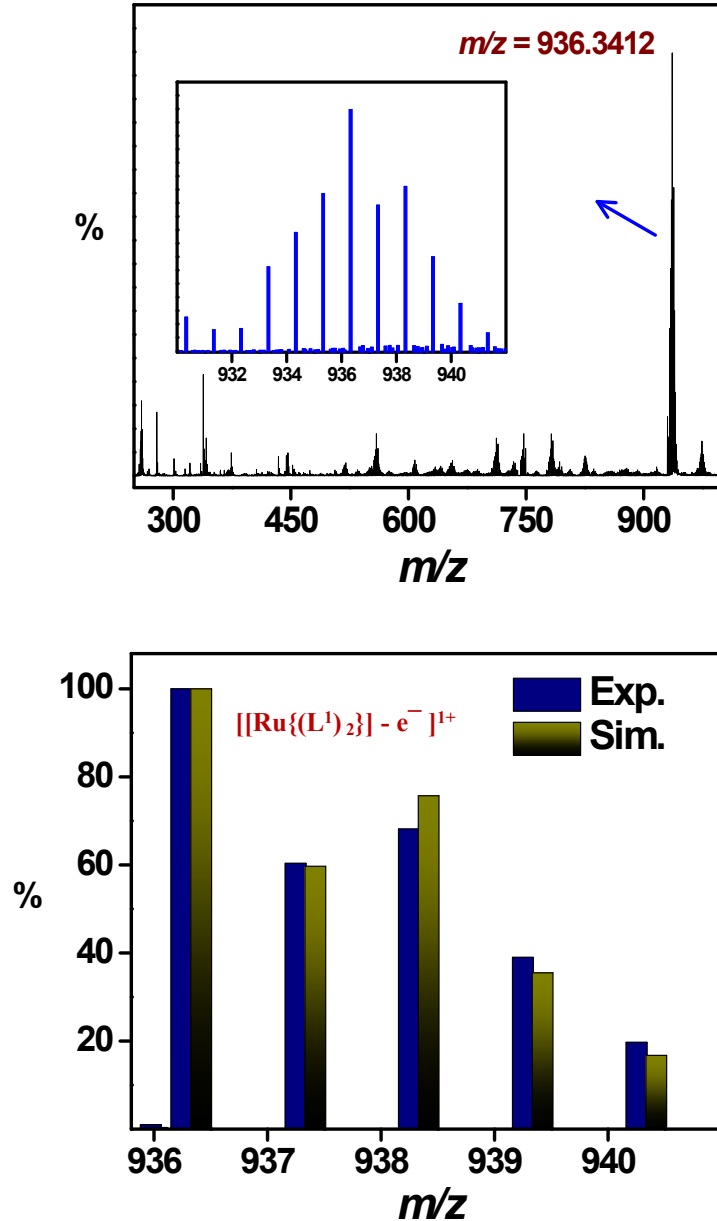
**Table S15** TD-DFT-calculated electronic transitions for **1**, using B3LYP

**Table S16** TD-DFT-calculated electronic transitions for  $[1^{OX1}]^{1+}$ , using CAM-B3LYP

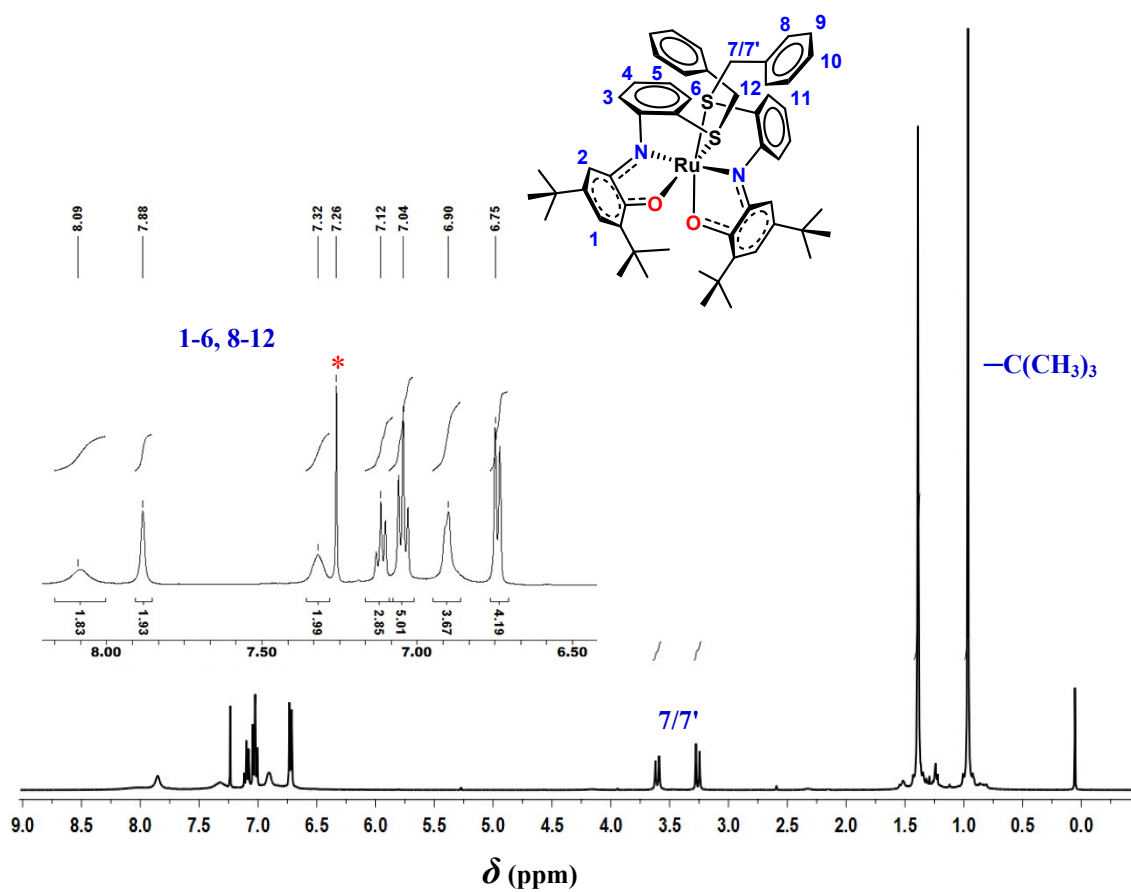
**Table S17** TD-DFT-calculated electronic transitions for  $[1^{OX1}]^{1+}$ , using B3LYP

**Table S18** TD-DFT-calculated electronic transitions for  $[1^{OX2}]^{2+}$ , using CAM-B3LYP

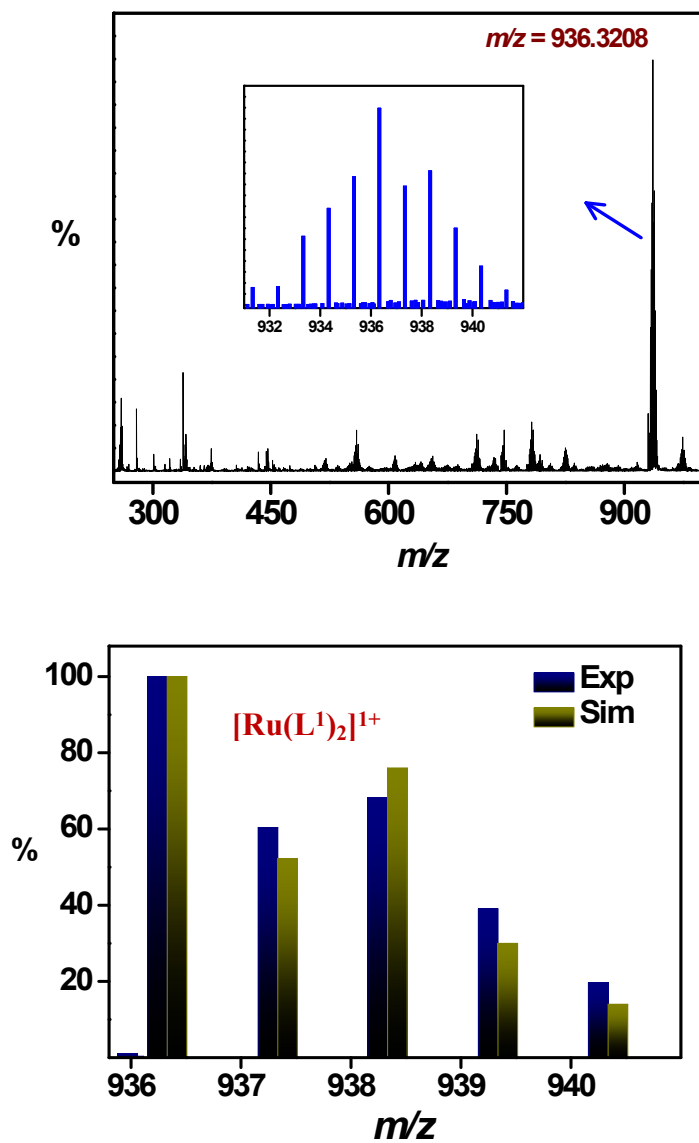
**Table S19** TD-DFT-calculated electronic transitions for  $[1^{OX2}]^{2+}$ , using B3LYP



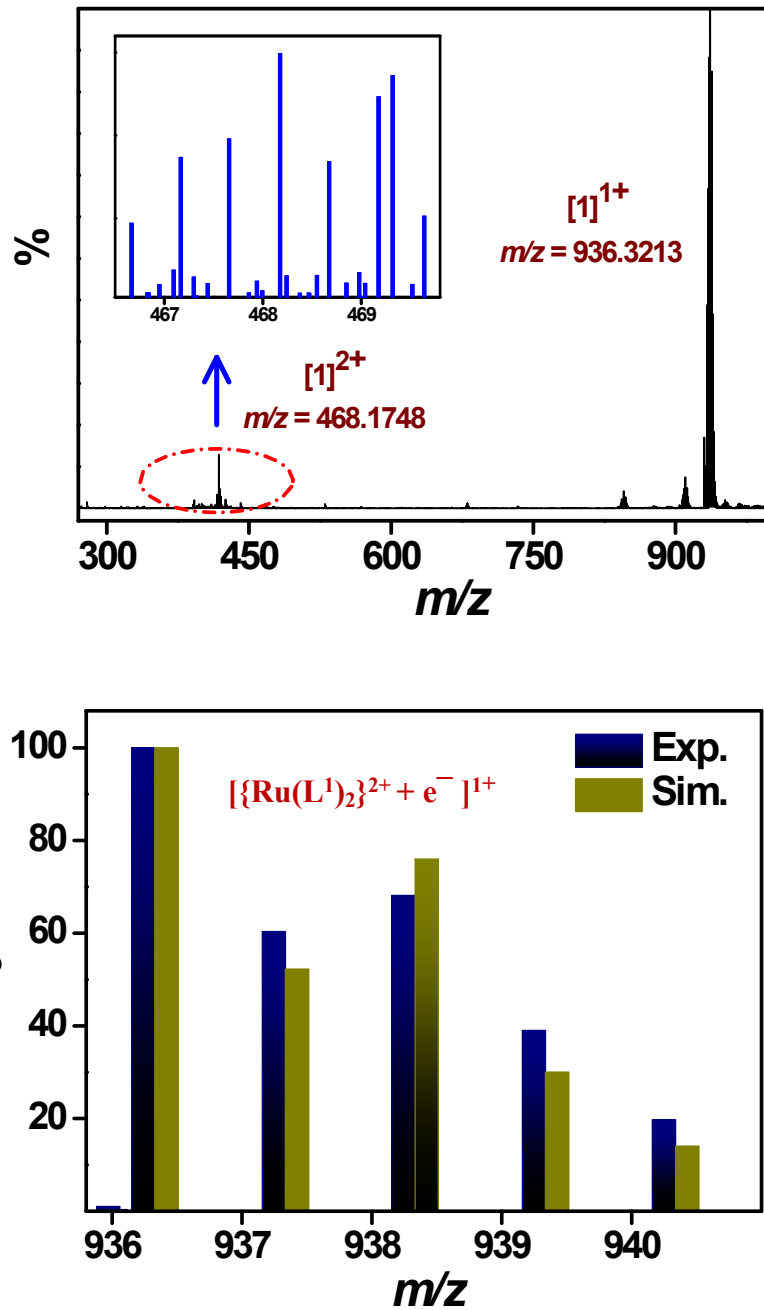
**Fig. S1** Positive-ion ESI-MS spectra of  $\{[Ru(L^1)_2] - e^- \}^{1+}$ .



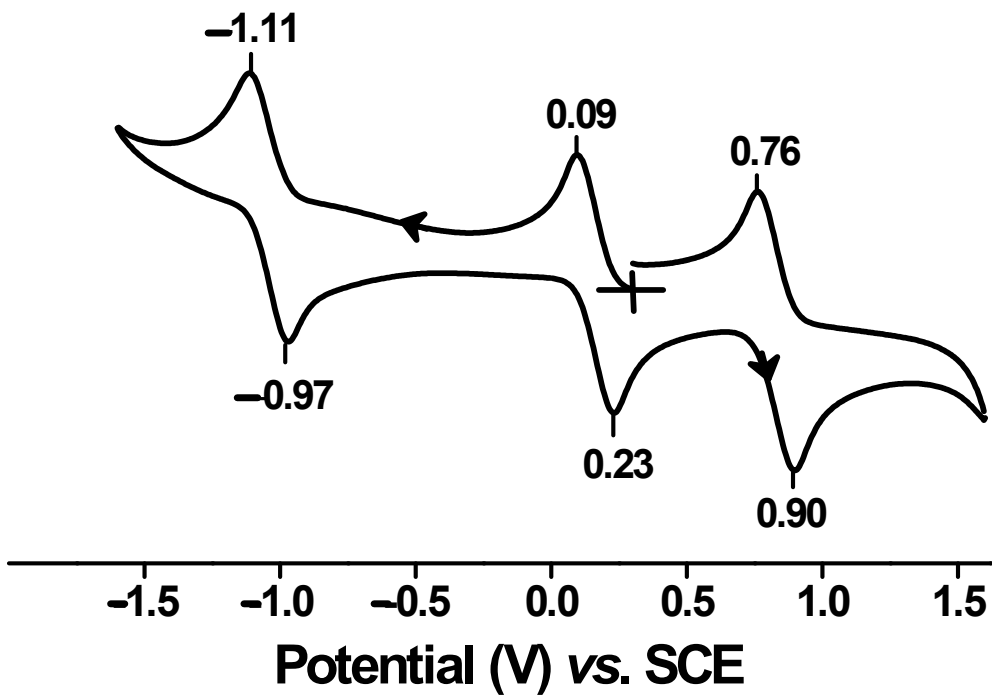
**Fig. S2**  $^1\text{H}$  NMR spectrum (400 MHz,  $\text{CDCl}_3$ ) of  $[\text{Ru}(\text{L}^1)_2]$  (**1**) at 298 K. Peak denoted by \* is due to residual  $\text{CHCl}_3$ .



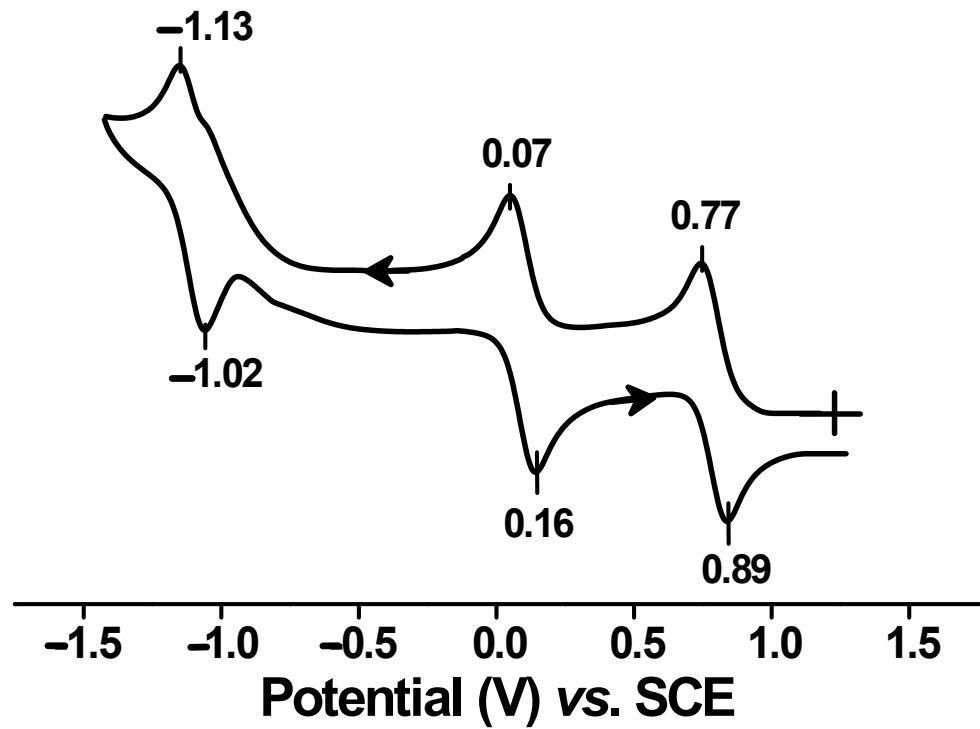
**Fig. S3** Positive-ion ESI-MS spectra of  $[\text{Ru}(\text{L}^1)_2]^{1+}$ .



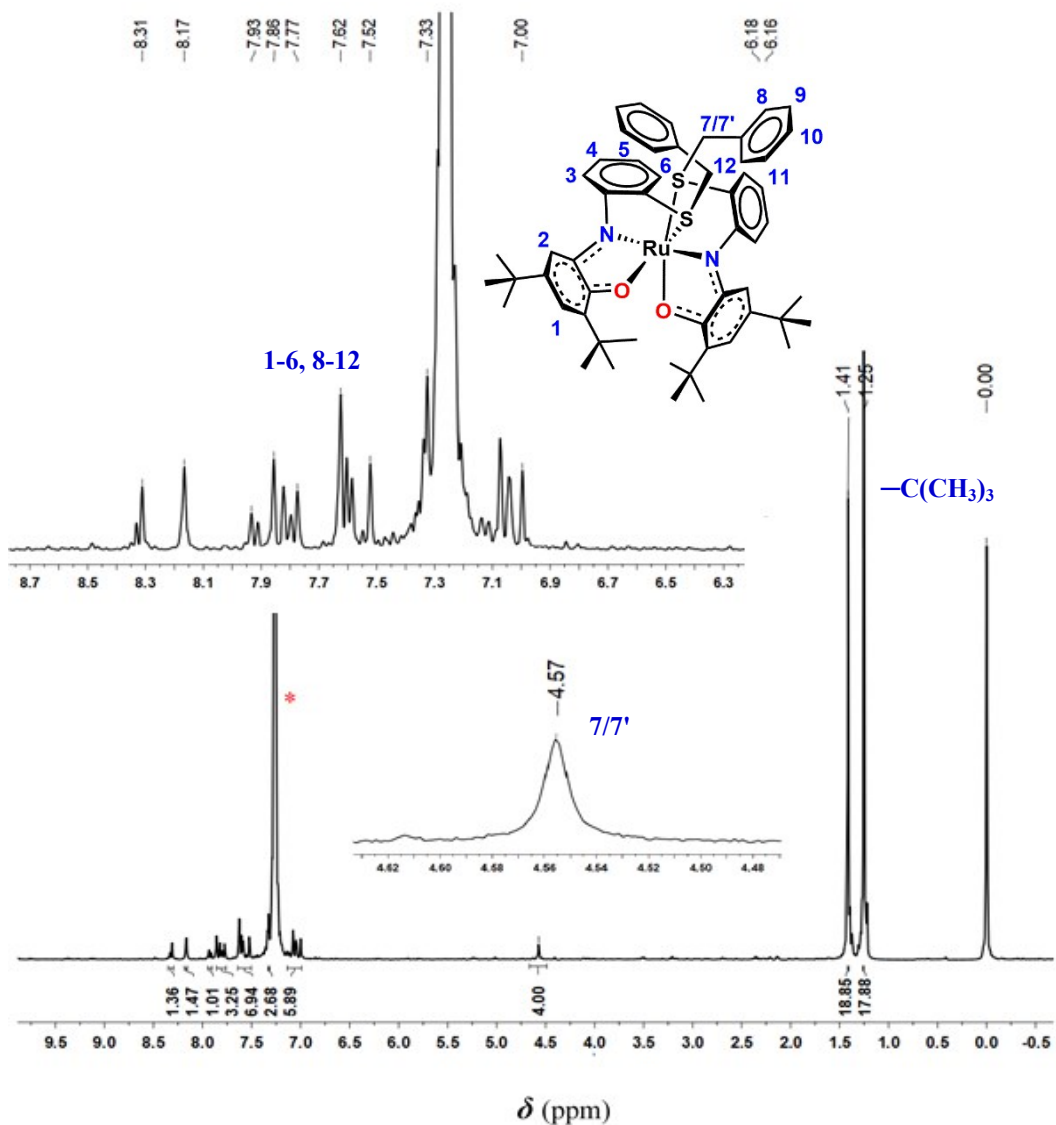
**Fig. S4** Positive-ion ESI-MS spectra of  $\{[Ru(L^1)_2]^{2+} + e^- \}^{1+}$ .



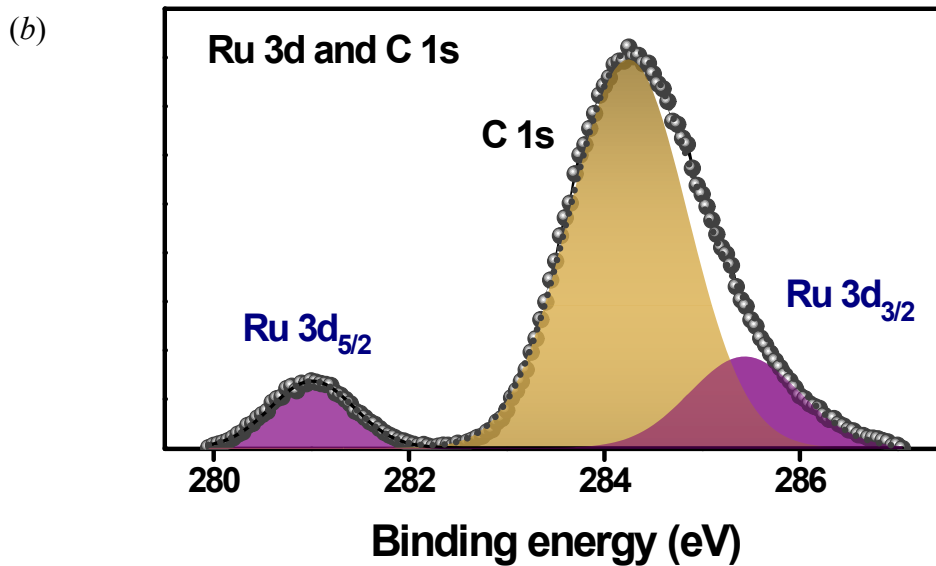
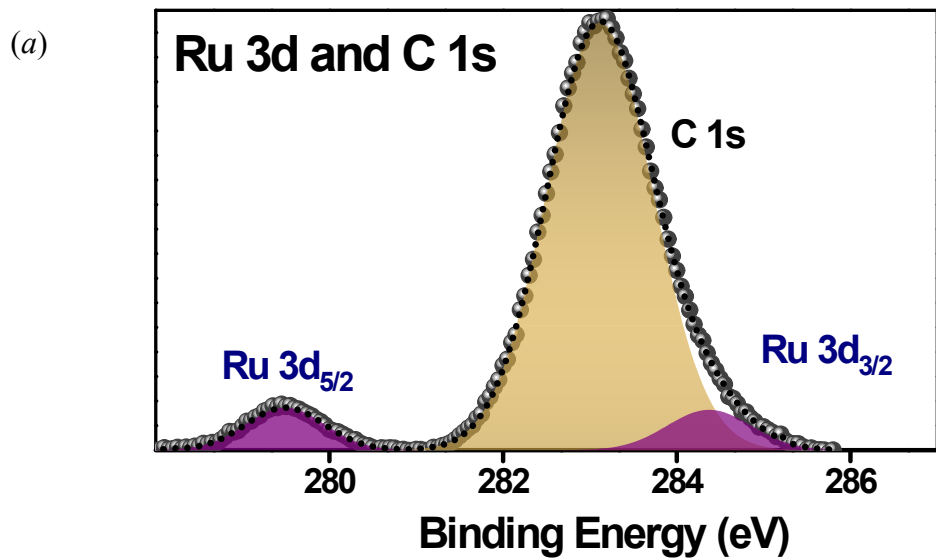
**Fig. S5** Cyclic voltammogram (100 mV/s) of a 0.5 mM solution of  $[1^{Ox1}](PF_6)\cdot CH_2Cl_2$  in  $CH_2Cl_2$  (0.1 M in TBAP) at a platinum working electrode. Indicated peak potentials are in V vs. SCE.

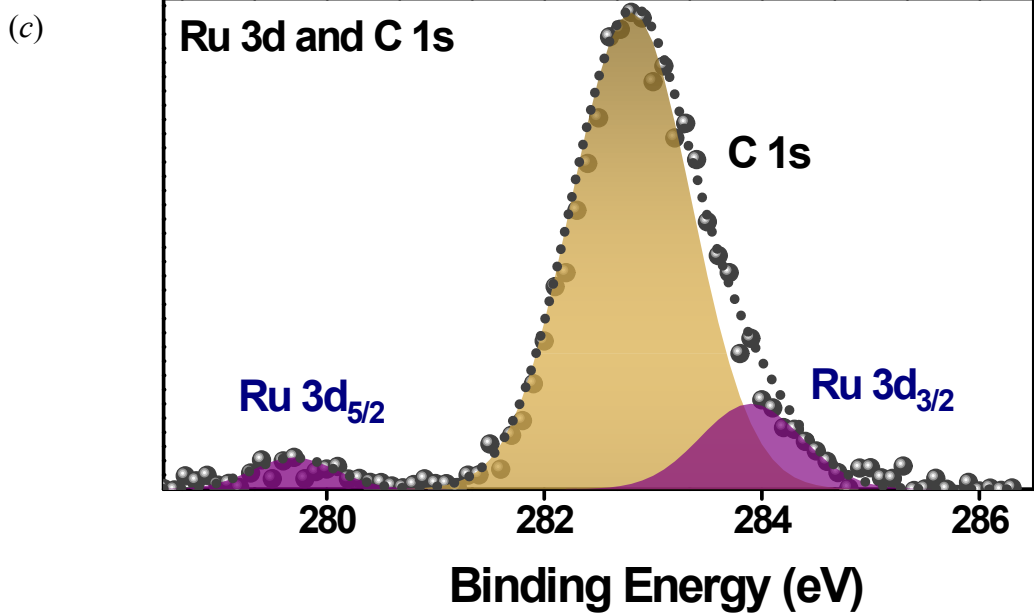


**Fig. S6** Cyclic voltammogram (100 mV/s) of a 0.5 mM solution of **3** / [**1<sup>OX2</sup>**]( $\text{BF}_4$ )<sub>2</sub>•H<sub>2</sub>O in CH<sub>2</sub>Cl<sub>2</sub> (0.1 M in TBAP) at a platinum working electrode. Indicated peak potentials are in V vs. SCE.

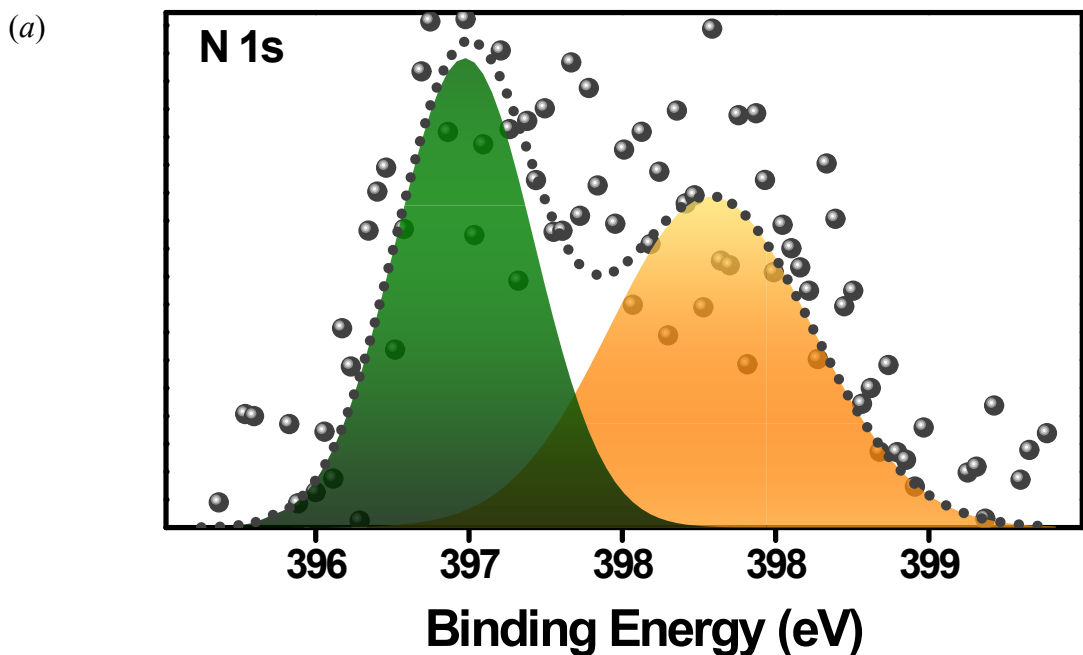


**Fig. S7**  $^1\text{H}$  NMR spectrum (400 MHz,  $\text{CDCl}_3$ ) of **3** /  $[\mathbf{1}^{\text{OX2}}](\text{BF}_4)_2 \cdot \text{H}_2\text{O}$  Peak denoted by \* is due to residual  $\text{CHCl}_3$ .





**Fig. S8** XPS of Ru 3d and C 1s core levels for (a) 1, (b) 2 and (c) 3, where yellow and purple lines represent C 1s and Ru 3d core level, respectively.



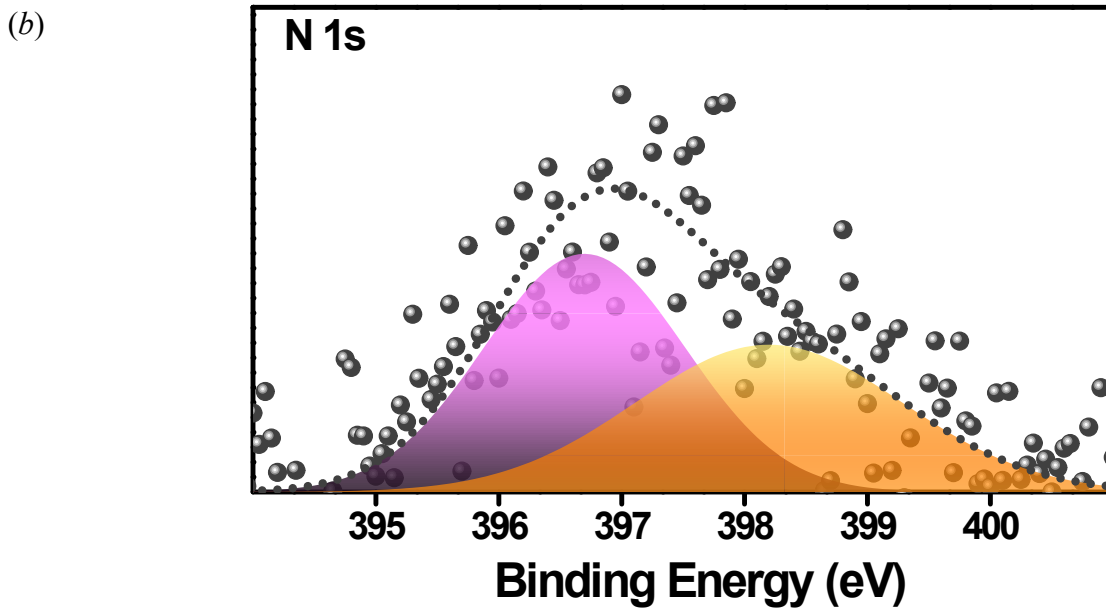


**Fig. S9** XPS of N 1s core level (*a*) for **1**, where yellow and green lines represent  $(L^{ISQ})^{\bullet-}$  and  $(L^{AP})^{2-}$  redox levels, respectively; (*b*) for **3**, where bluish pink and yellow lines represent  $(L^{IBQ})^0$  and  $(L^{ISQ})^{\bullet-}$  redox levels, respectively.

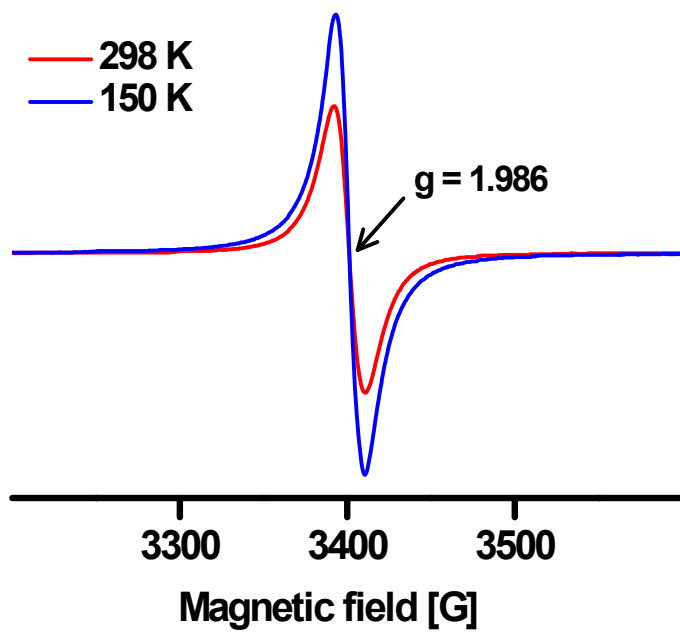


**Fig. S10** X-band EPR spectrum ( $\nu = 9.458$  GHz, power = 0.188 mW, receiver gain =  $1 \times 10^3$ , modulation frequency = 100 KHz, modulation amplitude = 1.00 G) recorded for solid  $[1^{OX1}](\text{PF}_6)\bullet\text{CH}_2\text{Cl}_2$  at 150 K and at 298 K.

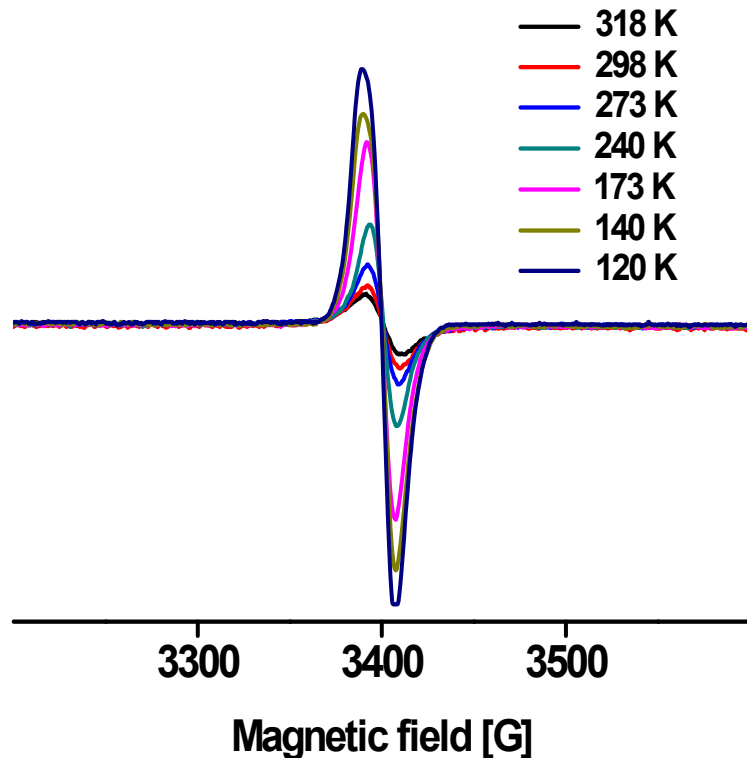


**Fig. S11** X-band EPR spectra ( $\nu = 9.458$  GHz, power = 0.188 mW, receiver gain =  $1 \times 10^3$ , modulation frequency = 100 KHz, modulation amplitude = 1.00 G) recorded for 1 mM solution of  $[1^{\text{Oxi}}]^{1+}$  in  $\text{CHCl}_3\text{-C}_6\text{H}_5\text{CH}_3$  (1:1, v/v) at variable temperatures (120 – 318 K).

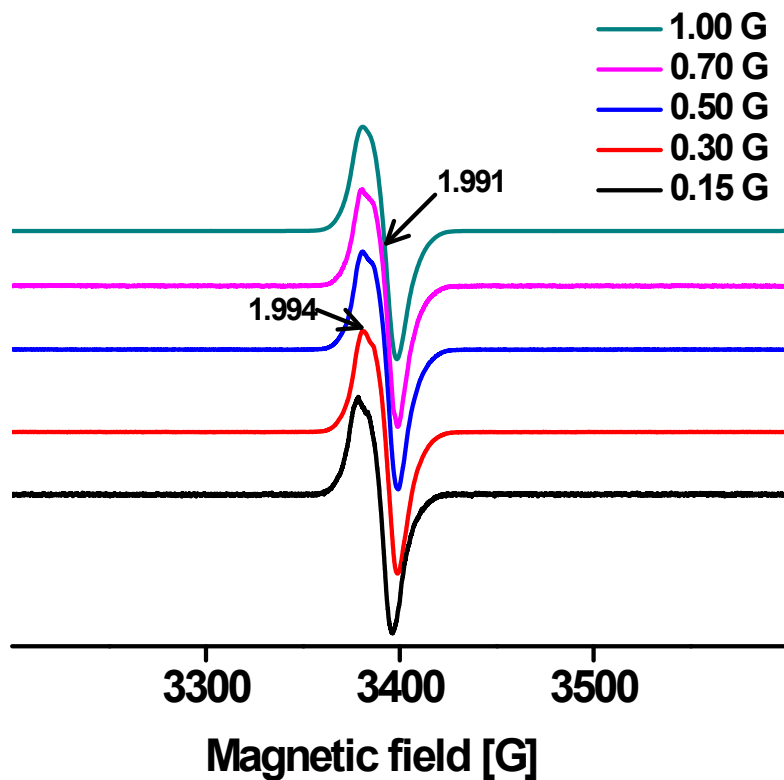


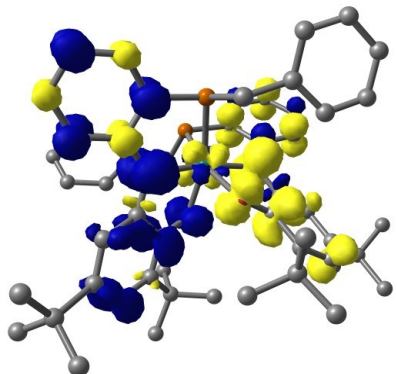
**Fig. S12** X-band EPR spectra ( $\nu = 9.458$  GHz, power = 0.188 mW, receiver gain =  $1 \times 10^3$ , modulation frequency = 100 KHz, modulation amplitude = 0.15–1.00 G) recorded for 1 mM solution of  $[1^{OX1}]^{1+}$  in  $\text{CHCl}_3\text{-C}_6\text{H}_5\text{CH}_3$  (1:1, v/v) at 120 K.

## Computational details

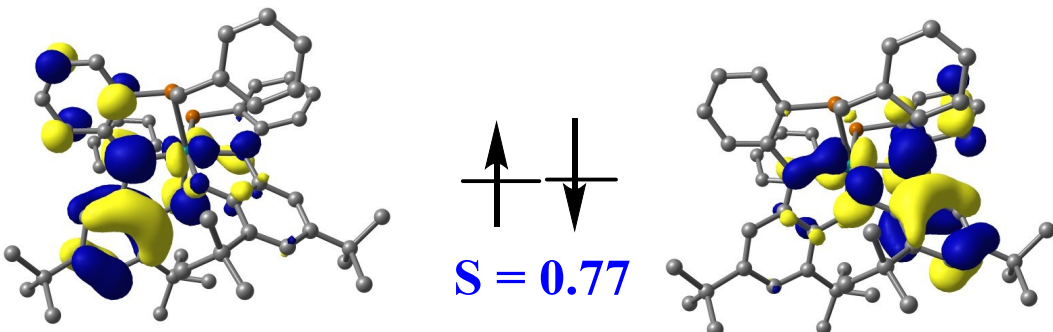
### **Spin population analysis**

All structural optimizations were employed using the Gaussian 09 program package<sup>1</sup> with a hybrid exchange-correlation functional Coulomb-Attenuating Method-B3LYP (CAM-B3LYP) as well as B3LYP (20% Hartree-Fock (HF) exchange admixture) functional for comparison.<sup>2-4</sup> For calculations, the quasi-relativistic effective core LANL2DZ pseudopotential<sup>5a</sup> and the corresponding optimized set of basis function was used for Ru. Valence double-zeta polarized basis-set 6-311+G(d)<sup>5b</sup> was employed for N, O, and S and 6-31G(d,p)<sup>5c</sup> basis-set was used for C and H. For spin-polarized symmetry-broken solution, the broken-symmetry formalism of Noddleman was used.<sup>6,7a</sup> The symmetry-broken,<sup>7</sup> singlet-diradical wave function of **1** and  $[1^{ox2}]^{2+}$  were optimized in Gaussian 09.<sup>1</sup> Initially, the stability analysis of the DFT wave functions were performed using the “stable=opt” keyword. The program will automatically find the lowest energy wave function if there is any symmetry-broken DFT solution. The spin-polarized broken-symmetry (BS) solutions of **1** and  $[1^{ox2}]^{2+}$  were performed by consequent optimization of the DFT wave function with high-spin triplet states ( $S_T = 1$ ), followed by geometry optimizations on the BS  $M_S = 0$  surface with “Guess=Mix” keyword.<sup>7b</sup> The symmetry broken solution is measured from the non-zero expectation value of the spin operator ( $\langle S^2 \rangle$ ). The energy differences between different states are represented as sum of electronic and zero-point energy with its zero

(a)



(b)



$232\alpha$   
 99 % L

$232\beta$   
 85 % L

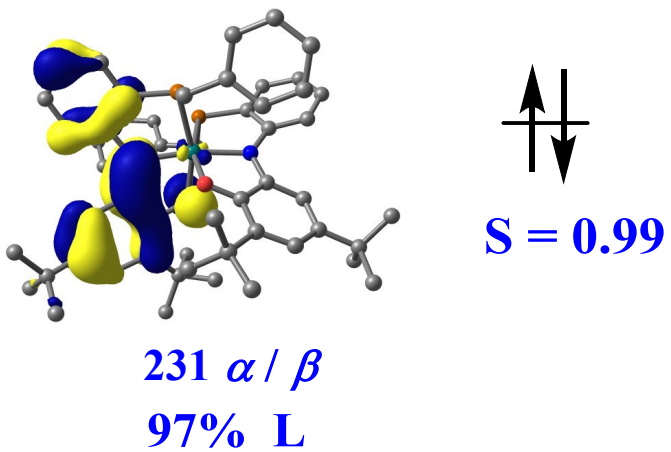


**Fig. S13** (a) Mulliken spin population and (b) qualitative MO diagram of the magnetic orbitals of **1** using CAM-B3LYP as functional.

point correction ( $\Delta E$ ). For the monocation  $[1^{OX1}]^{1+}$  the BS calculations were carried out following the same procedure mentioned above. We performed the vibrational frequency calculations on **1**,  $[1^{OX1}]^{1+}$  and  $[1^{OX2}]^{2+}$  at the same level to characterize their nature at energy minima. Mulliken atomic spin populations were also calculated at the optimized geometry. The wave functions of the optimized geometries for **1**, **2** and **3** (100 K data), excluding the counteranion(s) and solvent(s) of crystallization, were used for TD-DFT calculations employing both CAM-B3LYP and also B3LYP functional and the conductor-like polarizable continuum model CPCM (CH<sub>2</sub>Cl<sub>2</sub> as solvent).<sup>8</sup> TD-DFT-derived electronic spectra were plotted using GaussSum.<sup>9</sup> Corresponding orbitals and spin population plots were made using the Chemcraft,<sup>10</sup> visualization program.

**QRO analysis.** All calculations were performed using the ORCA quantum chemical program package<sup>11</sup> to understand the electronic structure of  $[Ru(L^1)_2]^{n+}$  ( $n = 0-2$ ). These calculations were performed at Azure computational facility at IIT Roorkee. To construct computational models for geometry optimization (Fig. S14, ESI†), large *tert*-butyl groups located at a distance away from the core have been truncated from the crystal structures (100 K) of **1**,  $[1^{OX1}]^{1+}$  (crystallized as  $[1^{OX1}](PF_6)\bullet CH_2Cl_2\bullet H_2O$  (**2**)), and  $[1^{OX2}]^{2+}$  (crystallized as  $[1^{OX2}](BF_4)_2\bullet 1.7H_2O$  (**3**)). In order to perform a systematic electronic-structure comparison of one-electron and two-electron oxidized species with **1**, the charged complexes,  $[1^{OX1}]^{1+}$  and  $[1^{OX2}]^{2+}$ , were considered without inclusion of the counteranion and solvent(s) of crystallization.

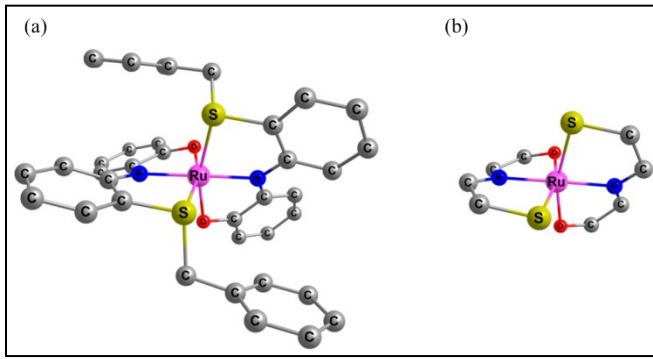


**Fig. S14** (a) Computational model system used for DFT calculations. Hydrogen atoms are not shown for clarity; (b) atoms for which def2-TZVP (-f) basis set is employed. For rest of the atoms def2-SVP basis set is used.

Geometries were optimized with the hybrid-GGA (generalized gradient approximation) density functional B3LYP<sup>2e,f,g</sup> in conjunction with def2-TZVP(-f) basis sets,<sup>12</sup> without f polarization functions for the first coordination sphere (Ru, O, C, N, and S) and def2-SVP basis sets<sup>13</sup> for the rest of the atoms (Fig. S14, ESI†). To accelerate the overall calculations, the RIJCOSX<sup>14</sup> (resolution-of-the-identity for Coulomb (RIJ) with a chain of sphere (COS) algorithm for the Hartree-Fock (HF) exchange (X) part) approximation was applied for the expensive integral calculations. Noncovalent interactions were accounted for by using atom-pairwise dispersion corrections with Becke-Johnson (D3BJ) damping.<sup>15</sup> Subsequent numerical frequency calculations were undertaken for the optimized geometries to confirm that they correspond to stationary points featuring no imaginary frequencies. The zero-point vibrational energies, thermal corrections, and entropy terms were obtained from the frequency calculations. Quasi restricted orbital (QRO)<sup>16</sup> analysis was performed using ORCA. QRO diagrams are visualized using the Chimera software.<sup>17</sup>

## References for computational details

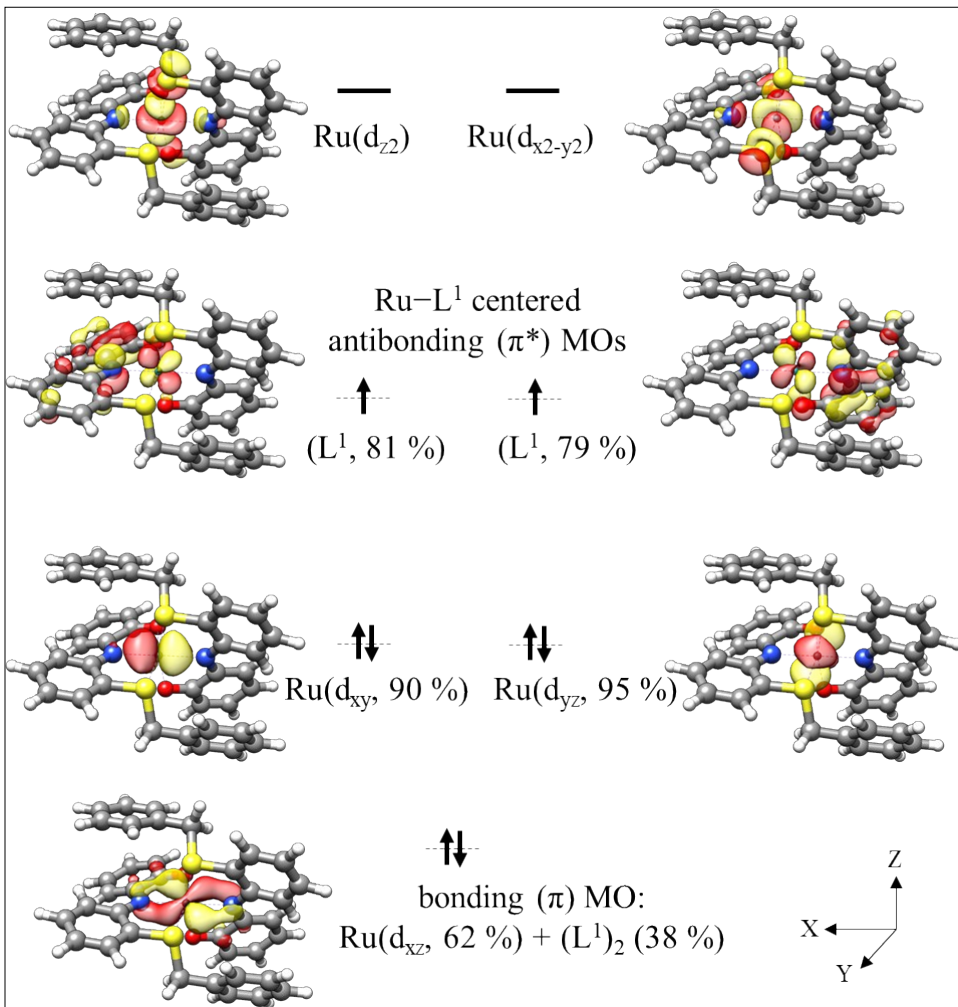
- (1) M. J. Frisch, G. W. Trucks, H. B. Schlegel, G. E.; Scuseria, M. A. Robb, J. R. Cheeseman, G. Scalmani, V. Barone, B. Mennucci, G. A. Petersson, H. Nakatsuji, M. Caricato, X. Li, H. P. Hratchian, A. F. Izmaylov, J. Bloino, G. Zheng, J. L. Sonnenberg, M. Hada, M. Ehara, K. Toyota, R. Fukuda, J. Hasegawa, M. Ishida, T. Nakajima, Y. Honda, O. Kitao, H. Nakai, T. Vreven, J. A. Jr. Montgomery, J. E. Peralta, F. Ogliaro, M. Bearpark, J. J. Heyd, E. Brothers, K. N.. Kudin, V. N. Staroverov, R. Kobayashi, J. Normand, K. Raghavachari, A. Rendell, J. C. Burant, S. S. Iyengar, J. Tomasi, M. Cossi, N. Rega, N. J. Millam, J. E. Klene, J. B. Knox, V. Cross, C. Bakken, J. Adamo, M. Jaramillo, R. Gomperts, R. E. Stratmann, O Yazyev, A. J. Austin, R. Cammi, C. Pomelli, J. W. Ochterski, R. L. Martin, K. Morokuma, V. G. Zakrzewski, G. A. Voth, P. Salvador, J. J. Dannenberg, S. Dapprich, A. D. Daniels, Ö. Farkas, J. B. Foresman, J. V. Ortiz, J. Cioslowski, D. J.; Fox, Gaussian 09, revision B.01; Gaussian, Inc.: Wallingford, CT, **2010**.
- (2) (a) I. V. Rostov, R. D. Amos, R. Kobayashi, G. Scalmani and M. J. Frisch, *J. Phys. Chem. B.*, 2010, **114**, 5547-5555; (b) D. Jacquemin, C. Michaux, E. A. Perpete, F. Maurel and A. Perrier, *Chem. Phys. Lett.*, 2010, **488**, 193-197; (c) D. Jacquemin, E. A. Perpete, G. E. Scuseria, I. Ciofini and C. Adamo, *J. Chem. Theory Comput.* 2008, **4**, 123-135; (d) M. M. Mikolajczyk, R. Zalesny, Z. Czyzniowska, P. Toman, J. Leszczynski and W. Bartkowiak, *J. Mol. Model.*, 2011, **17**, 2143-2149; (e) A. D. Becke, *Phys. Rev. A: At., Mol., Opt. Phys.*, 1988, **38**, 3098–3100; (f) A. D. Becke, *J. Chem. Phys.*, 1993, **98**, 5648–5652; (g) C. Lee, W. Yang and R. G. Parr, *Phys. Rev. B: Condens. Matter Mater. Phys.*, 1988, **37**, 785–789.

- (3) C. Remenyl and M. Kaupp, *J. Am. Chem. Soc.*, 2005, **127**, 11399–11413.
- (4) (a) Y. Yanai, D. P. Tew and N. C. Handy, *Chem. Phys. Lett.*, 2004, **393**, 51–57; (b) L. Chiang, A. Kochem, O. Jarjayes, T. J. Dunn, H. Vezin, M. Sakaguchi, T. Ogura, M. Orio, Y. Shimazaki, F. Thomas and T. Storr, *Chem. Eur. J.*, 2012, **18**, 14117–14127; (c) Y. Tawada, T. Tsuneda, S. Yanagisawa, T. Yanai and K. Hirao, *J. Chem. Phys.*, 2004, **120**, 8425–8433.
- (5) (a) P. J. Hay and W. R. Wadt, *J. Chem. Phys.*, 1985, **82**, 270–283; (b) G. A. Peterson, A. Bennett, T. G. Tensfeldt, M. A. Al-Laham, W. A. Shirley and J. Mantzaris, *J. Chem. Phys.*, 1988, **89**, 2193–2218; (c) G. A. Peterson and M. A. Al-Laham, *J. Chem. Phys.*, 1991, **94**, 6081–6090.
- (6) (a) P. A. Ginsberg, *J. Am. Chem. Soc.*, 1980, **102**, 111–117; (b) L. Noodleman and J. G. Jr. Norman, *J. Chem. Phys.*, 1979, **70**, 4903–4906; (c) L. Noodleman, *J. Chem. Phys.*, 1981, **74**, 5737–5743; (d) L. Noodleman and E. R. Davidson, *Chem. Phys.*, 1986, **109**, 131–143.
- (7) (a) V. Bachler, G. Olbrich, F. Neese and K. Wieghardt, *Inorg. Chem.*, 2002, **41**, 4179–4193; (b) Y. G. Park, M. F. Qayyum, J. Woertink, K. O. Hodgson, B. Hedman, A. A. N. Sarjeant, E. I. Solomon and K. D. Karlin, *J. Am. Chem. Soc.*, 2012, **134**, 8513–8524.
- (8) (a) V. Barone and M. Cossi, *J. Phys. Chem. A*, 1998, **102**, 1995–2001; (b) M. Cossi and V. Barone, *J. Chem. Phys.*, 2001, **115**, 4708–4717; (c) M. Cossi, N. Rega, G. Scalmani and V. Barone, *J. Comput. Chem.*, 2003, **24**, 669–681.
- (9) N. M. O’Boyle, A. L. Tenderholt, K. M. Langner, *J. Comput. Chem.*, 2008, **29**, 839–845.

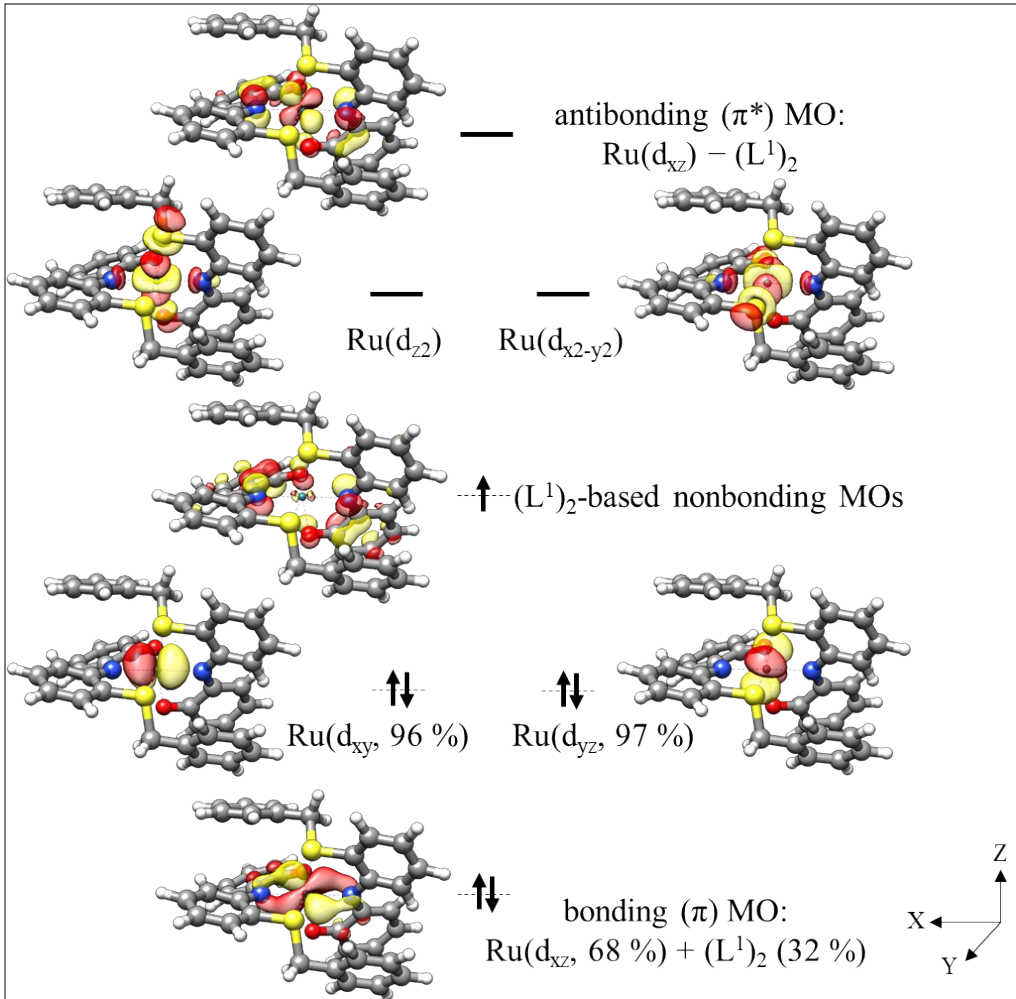
- (10) Chemcraft Visualization Program. <http://www.chemcraftprog.com/>.
- (11) F. Neese, The ORCA program system. *WIREs Comput. Mol. Sci.*, 2012, **2**, 73–78.
- (12) A. Schäfer, C. Huber and R. Ahlrichs, *J. Chem. Phys.*, 1994, **100**, 5829–5835.
- (13) A. Schäfer, H. Horn and R. Ahlrichs, *J. Chem. Phys.*, 1992, **97**, 2571–2577.
- (14) F. Neese, F. Wennmohs, A. Hansen and U. Becker, *Chem. Phys.*, 2009, **356**, 98–109.
- (15) S. Grimme, S. Ehrlich and L. Goerigk, *J. Comput. Chem.*, 2011, **32**, 1456–1465.
- (16) F. Neese, *J. Am. Chem. Soc.*, 2006, **128**, 10213–10222.
- (17) E. F. Pettersen, T. D. Goddard, C. C. Huang, G. S. Couch, D. M. Greenblatt, E. C. Meng and T. E. Ferrin, *J. Comput. Chem.*, 2004, **25**, 1605–1612.

---

**[Ru(L<sup>1</sup>)<sub>2</sub>] (S = 1, triplet).** In the triplet case (Fig. S15, ESI†) the two unpaired electrons are located in the Ru–L<sup>1</sup> centered antibonding ( $\pi^*$ ) orbitals, which are vacant in the case of closed-shell system. This implies that the triplet-state would be destabilized relative to the closed-shell species. In fact, the triplet state is found to be higher in energy ( $\Delta G = 5.2$  kcal/mol) than the closed-shell structure.



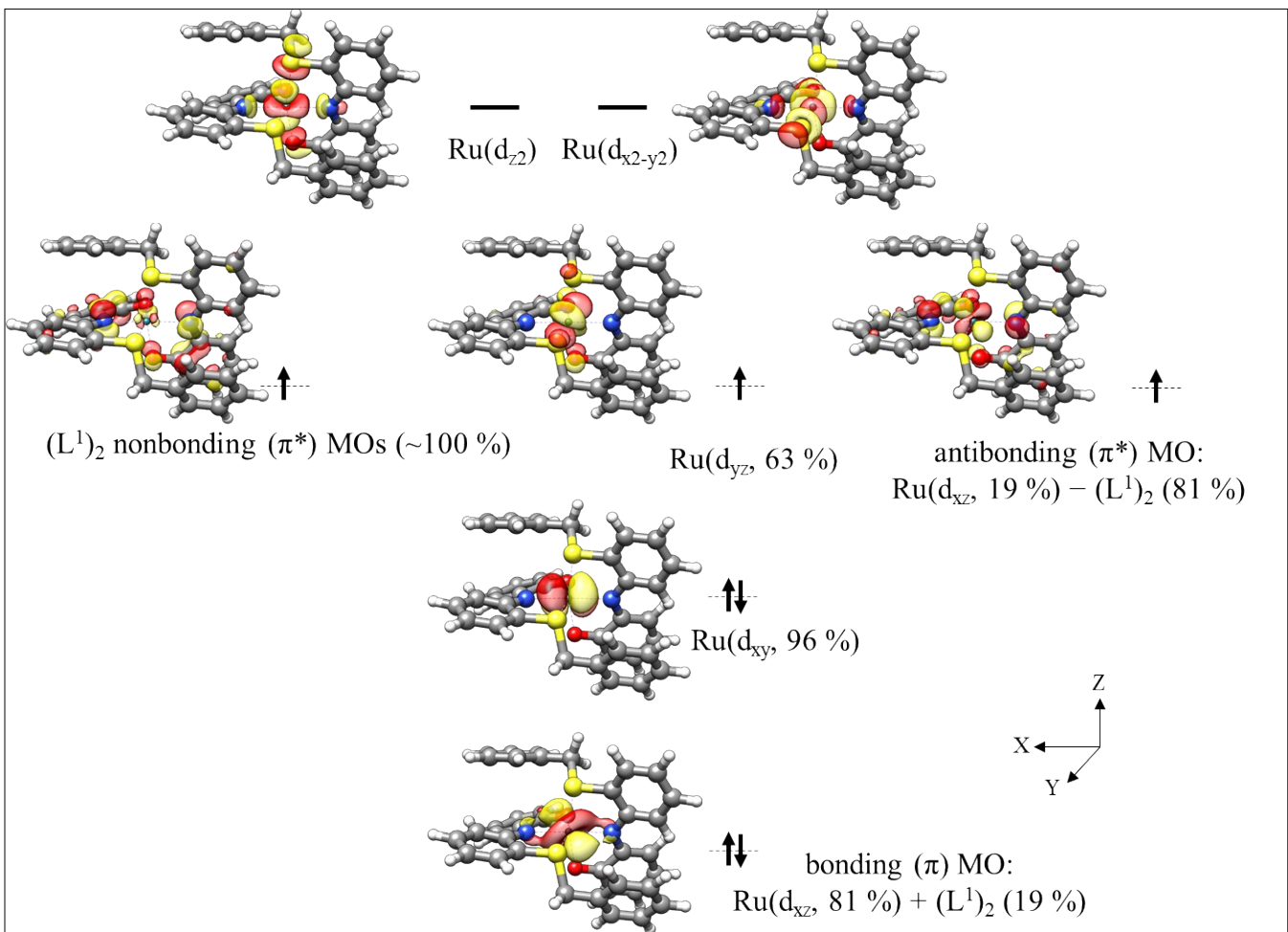
**Fig. S15** Qualitative frontier MO diagram of  $[\text{Ru}(\text{L}^1)_2]$  ( $S = 1$ ) obtained from its unrestricted Kohn-Sham geometry-optimized structure.



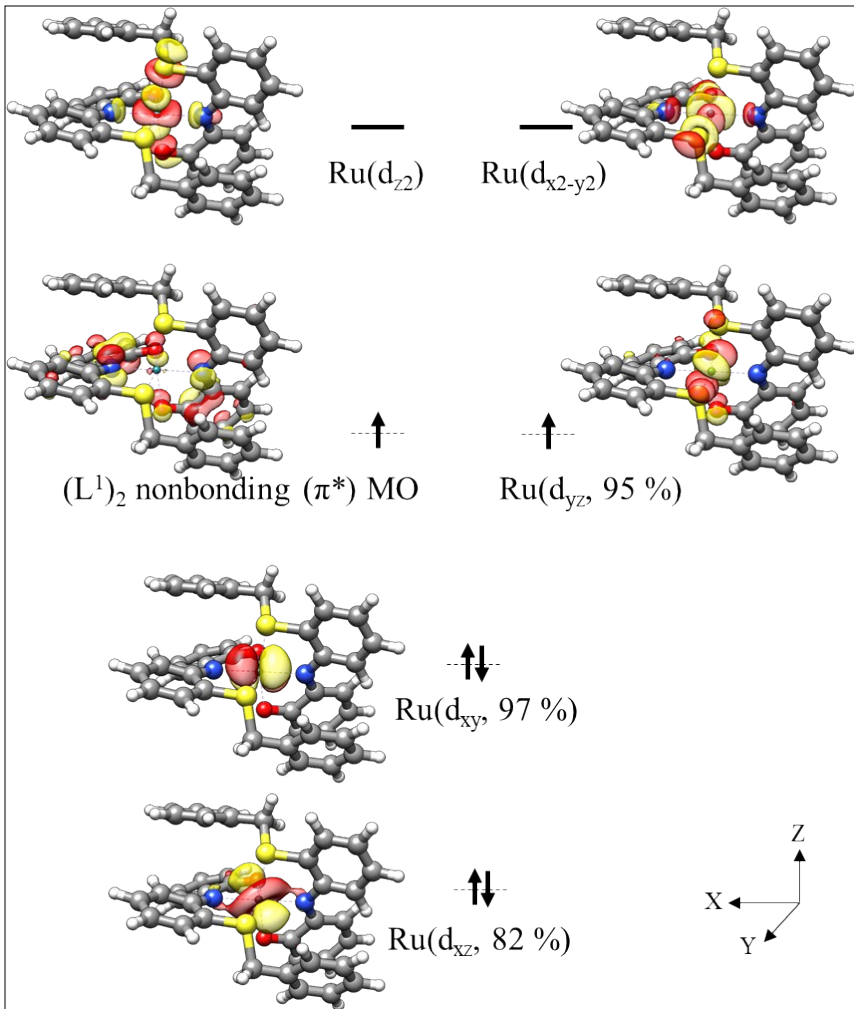
**Fig. S16** Qualitative QRO diagram of  $[\text{Ru}(\text{L}^1)_2]^{1+}$  ( $S = 1/2$ , B3LYP).

**$[\text{Ru}(\text{L}^1)_2]^{1+}$  ( $S = 3/2$ , quartet).** The results for  $S = 3/2$  are presented in Fig. S17, ESI†.

Out of three unpaired electrons, one occupies in an antibonding ( $\text{Ru-d}_{xz} - \text{L}^1$  ligands) orbital and the other two are located in a ligand-based nonbonding and  $\text{Ru}(\text{d}_{yz})$  orbital, respectively. As the electrons are in the antibonding and nonbonding orbitals the geometry with  $S = 3/2$  would not be preferred over  $S = 1/2$  state, in which there is no electron in the antibonding orbital. DFT-based energy calculations show that indeed the doublet is more stable ( $\Delta G = 14$  kcal/mol) than the quartet state.

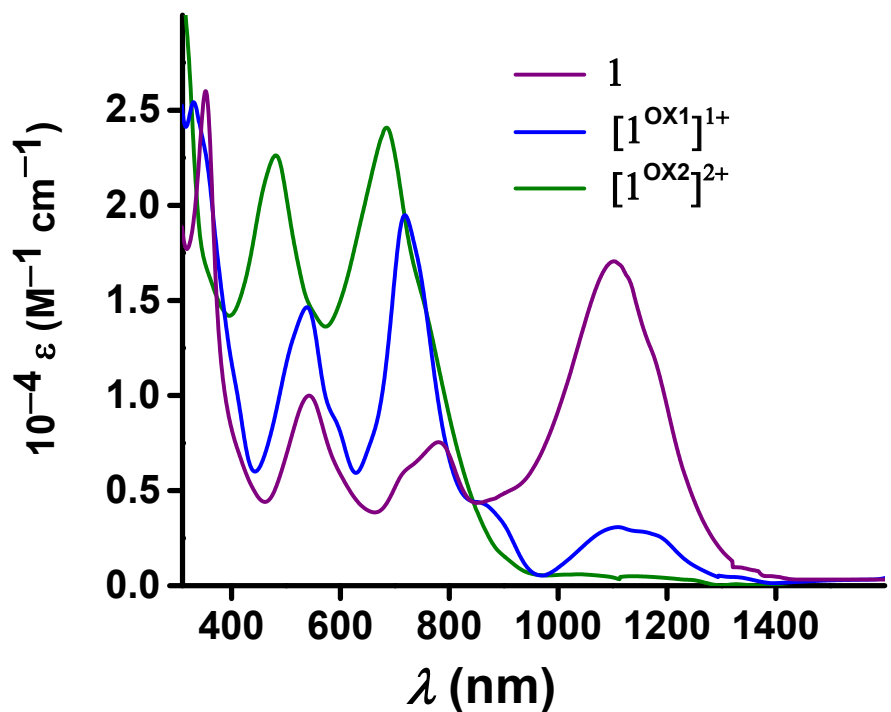


**Fig. S17** Qualitative frontier MO diagram for  $[\text{Ru}(\text{L}^1)_2]^{1+}$  ( $S = 3/2$ ).

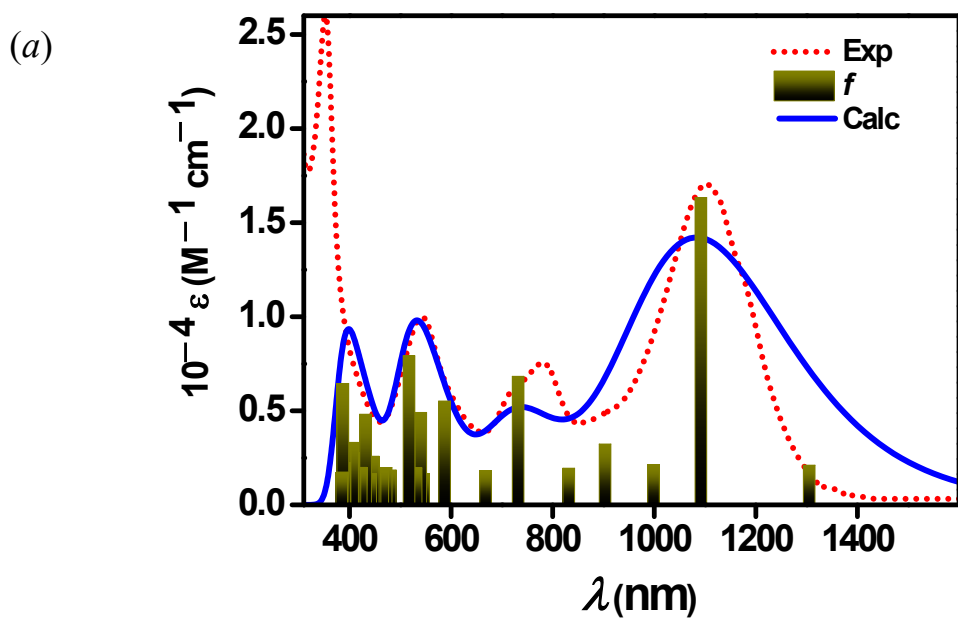


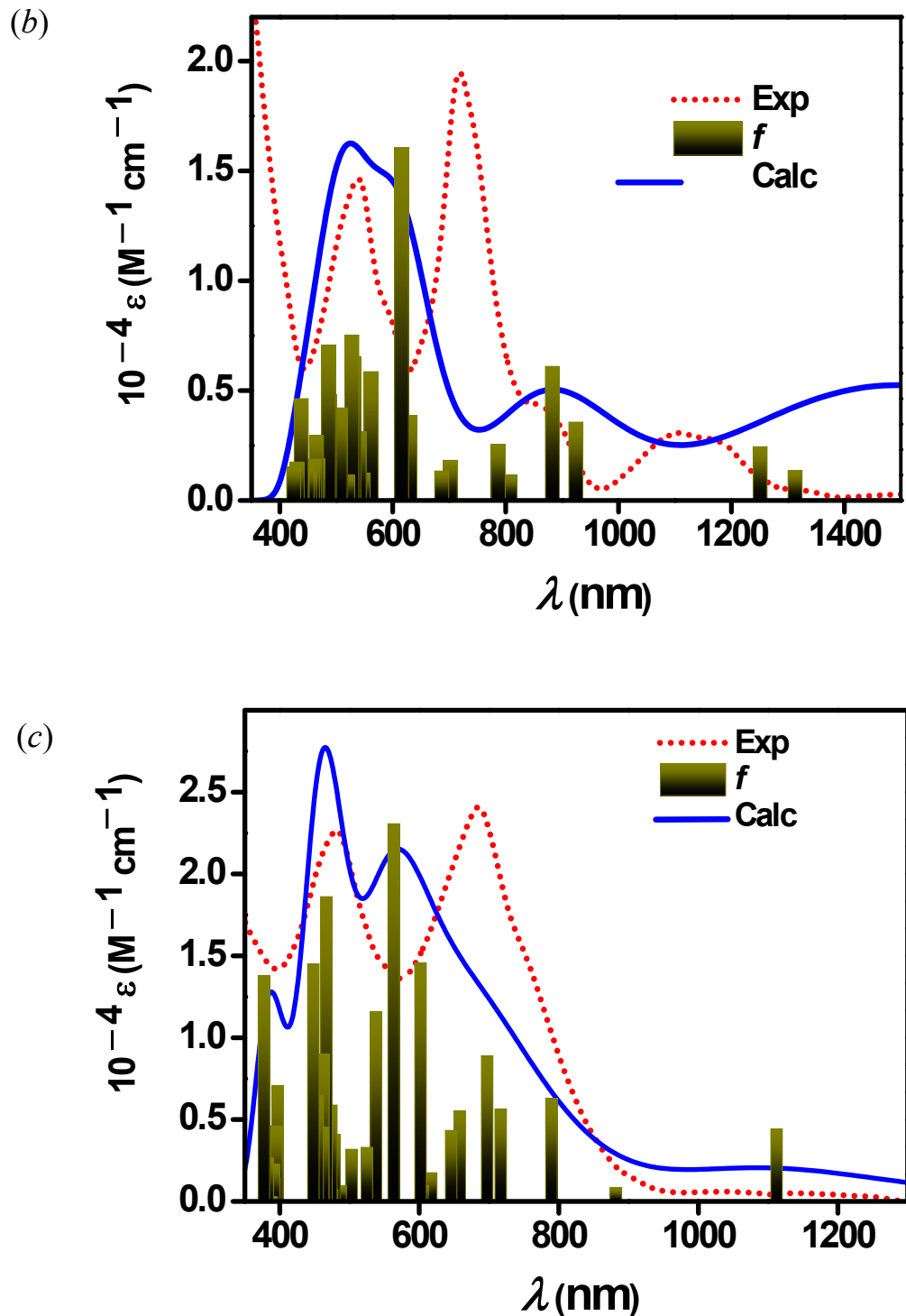
**Fig. S18** Qualitative frontier MO diagram for  $[\text{Ru}(\text{L}^1)_2]^{2+}$  ( $S = 1$ ).

**[ $\text{Ru}(\text{L}^1)_2]^{2+}$  ( $S = 1$ , triplet).** We have also studied the electronic structure of  $[\text{Ru}(\text{L}^1)_2]^{2+}$  with  $S = 1$  (Fig. S18, ESI†). Clearly, in the triplet state one unpaired electron is in the nonbonding orbital and the other in the Ru  $d_{yz}$  orbital, whereas in the CSS both electrons are in the Ru  $d_{yz}$  orbital. The triplet is less stable ( $\Delta G = 9$  kcal/mol) than the closed-shell species.

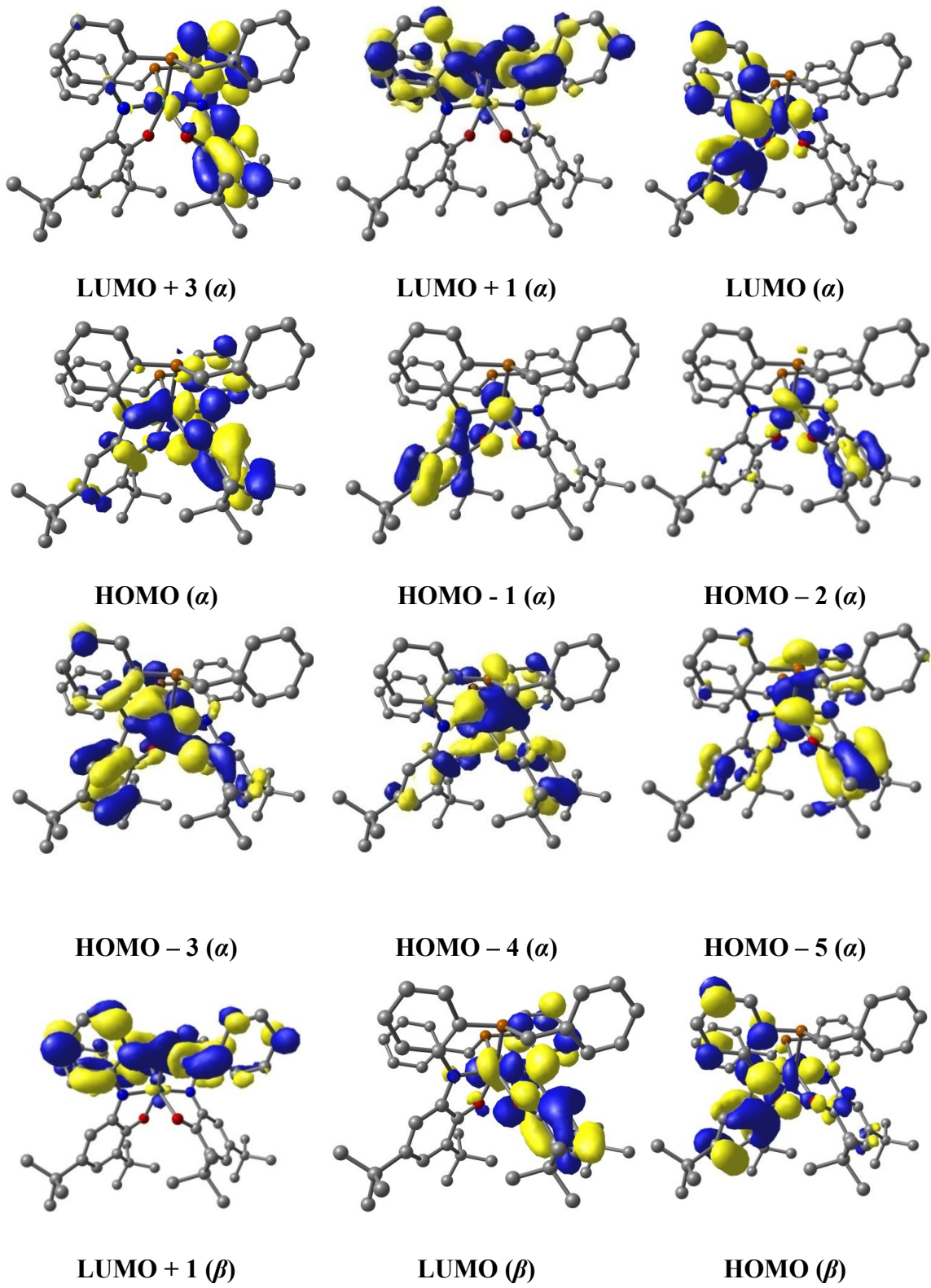


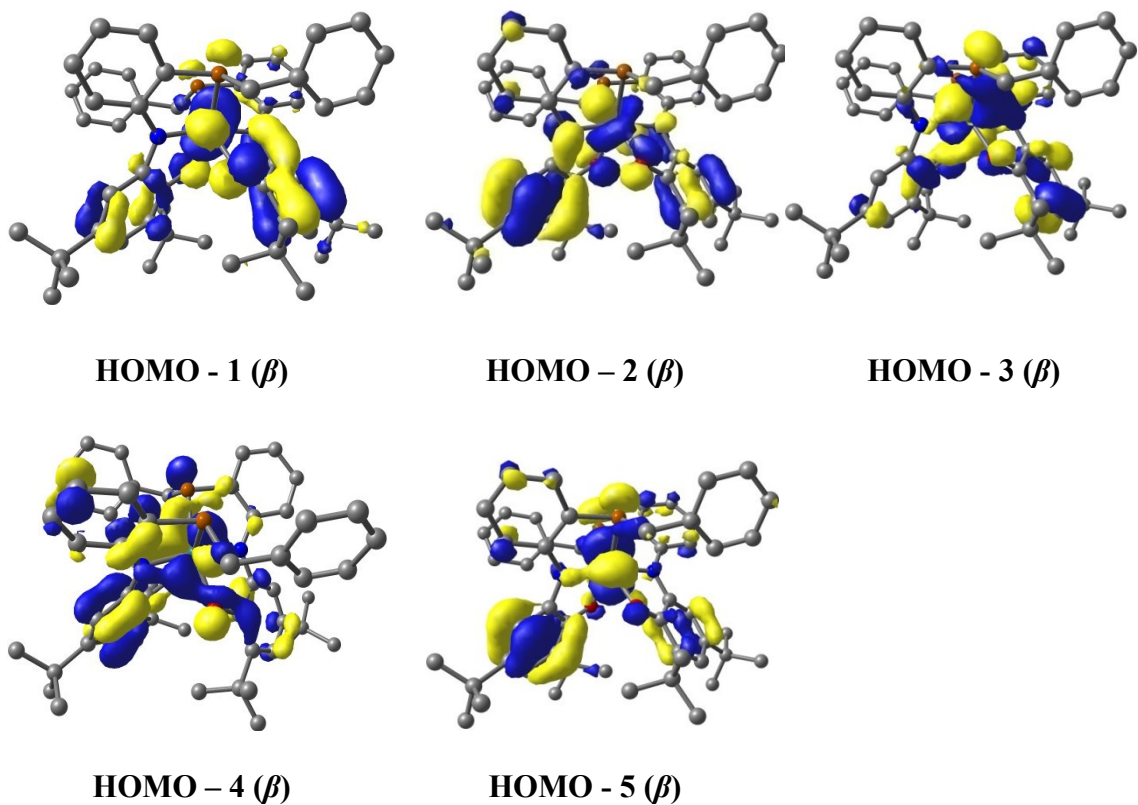
**Fig. S19** Electronic spectra of **1**,  $[1^{\text{OX1}}]^{1+}$ , and  $[1^{\text{OX2}}]^{2+}$  in  $\text{CH}_2\text{Cl}_2$  at 298 K.



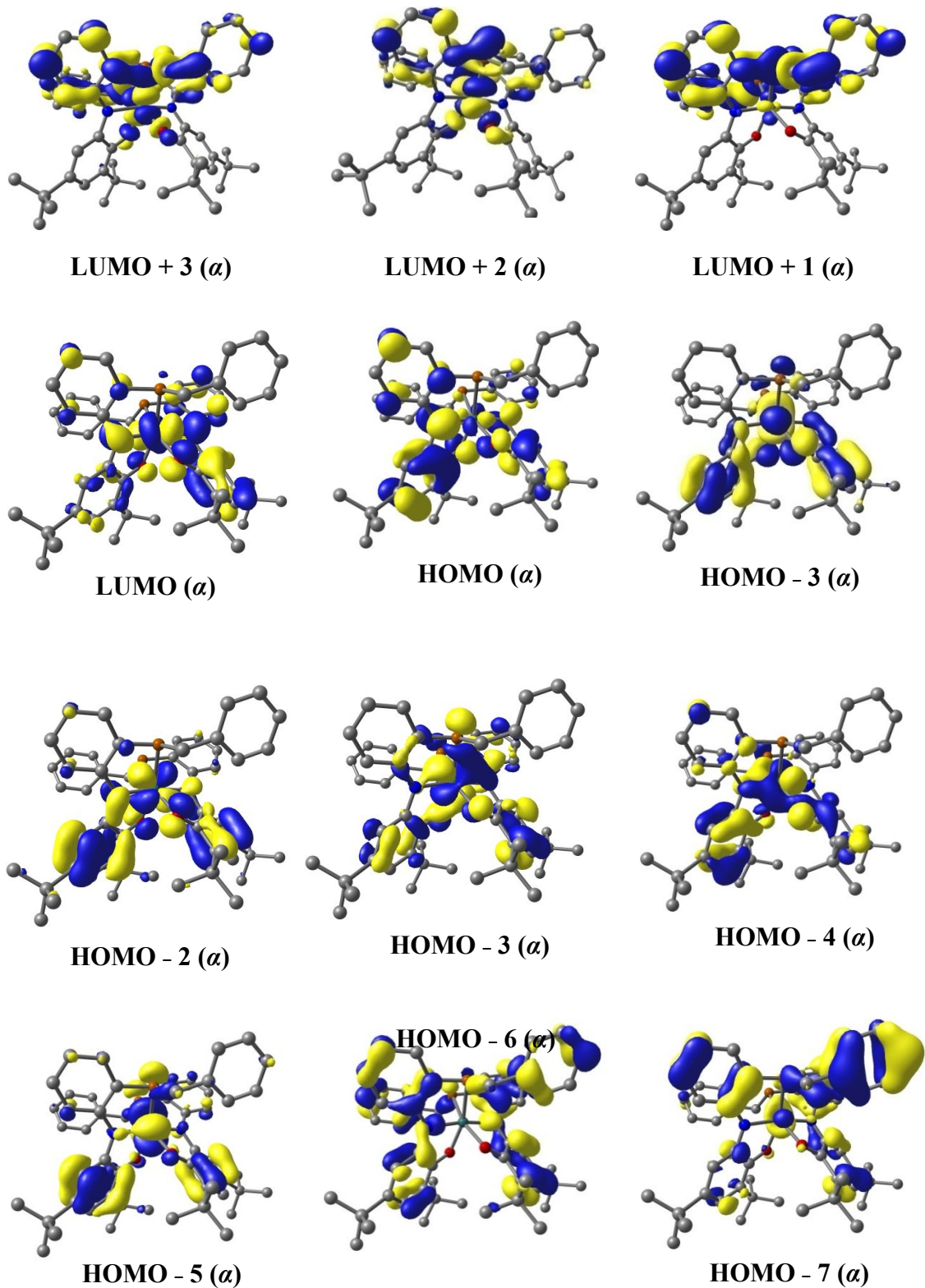


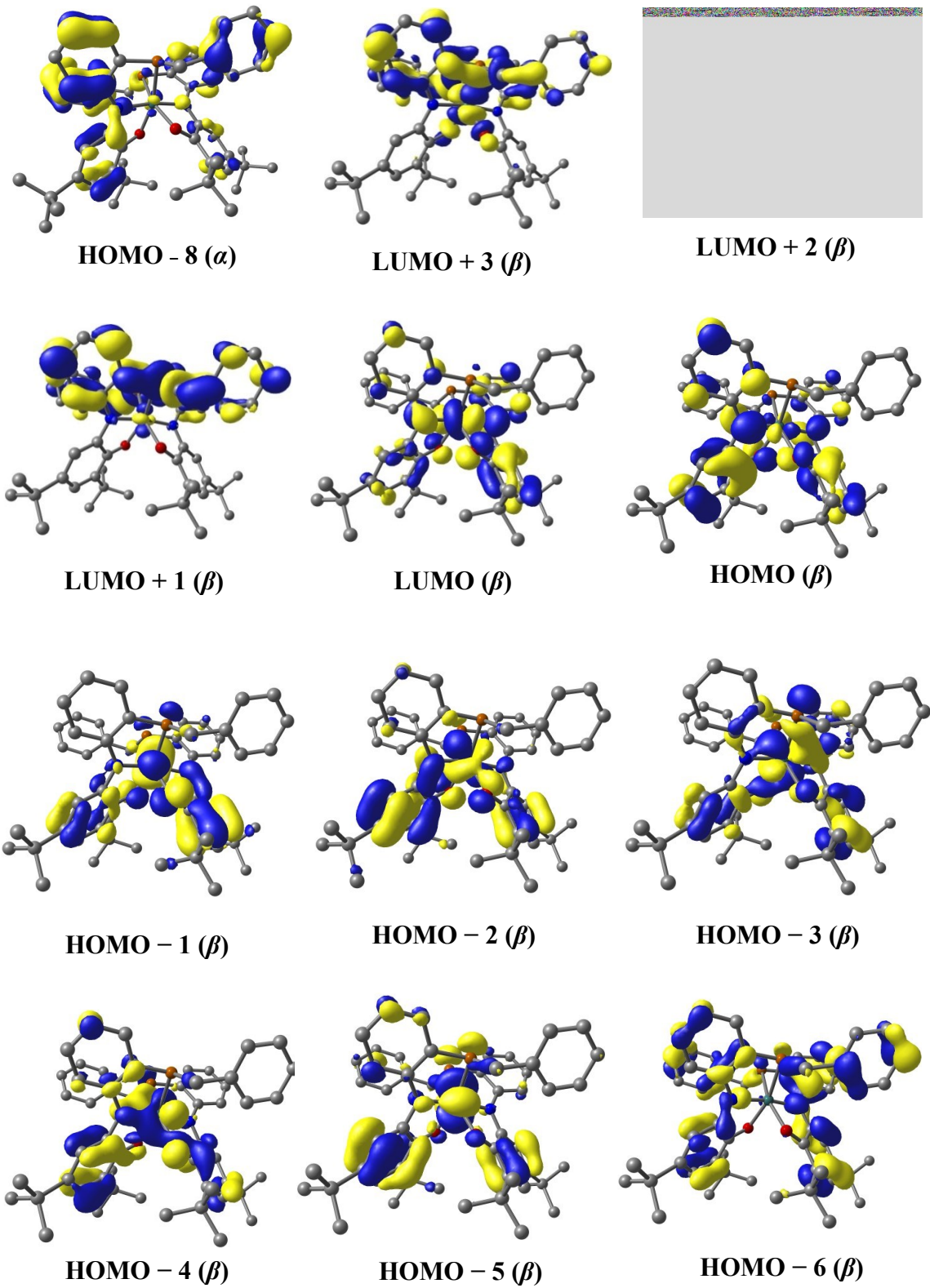
**Fig. S20** TD-DFT-Calculated electronic spectra of (a) 1, (b)  $[1^{\text{OX1}}]^{1+}$  and (c)  $[1^{\text{OX2}}]^{2+}$  using B3LYP level of theory.

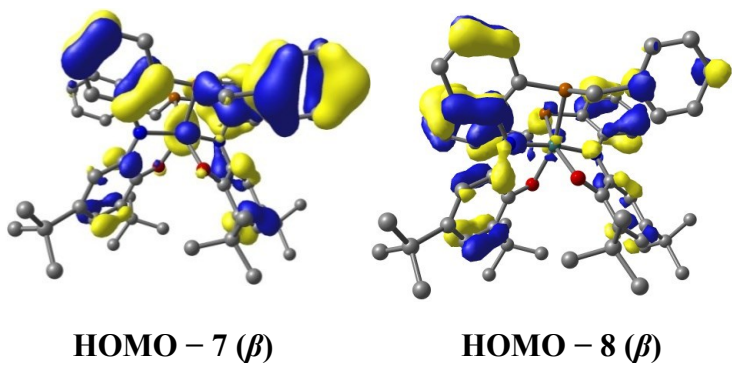




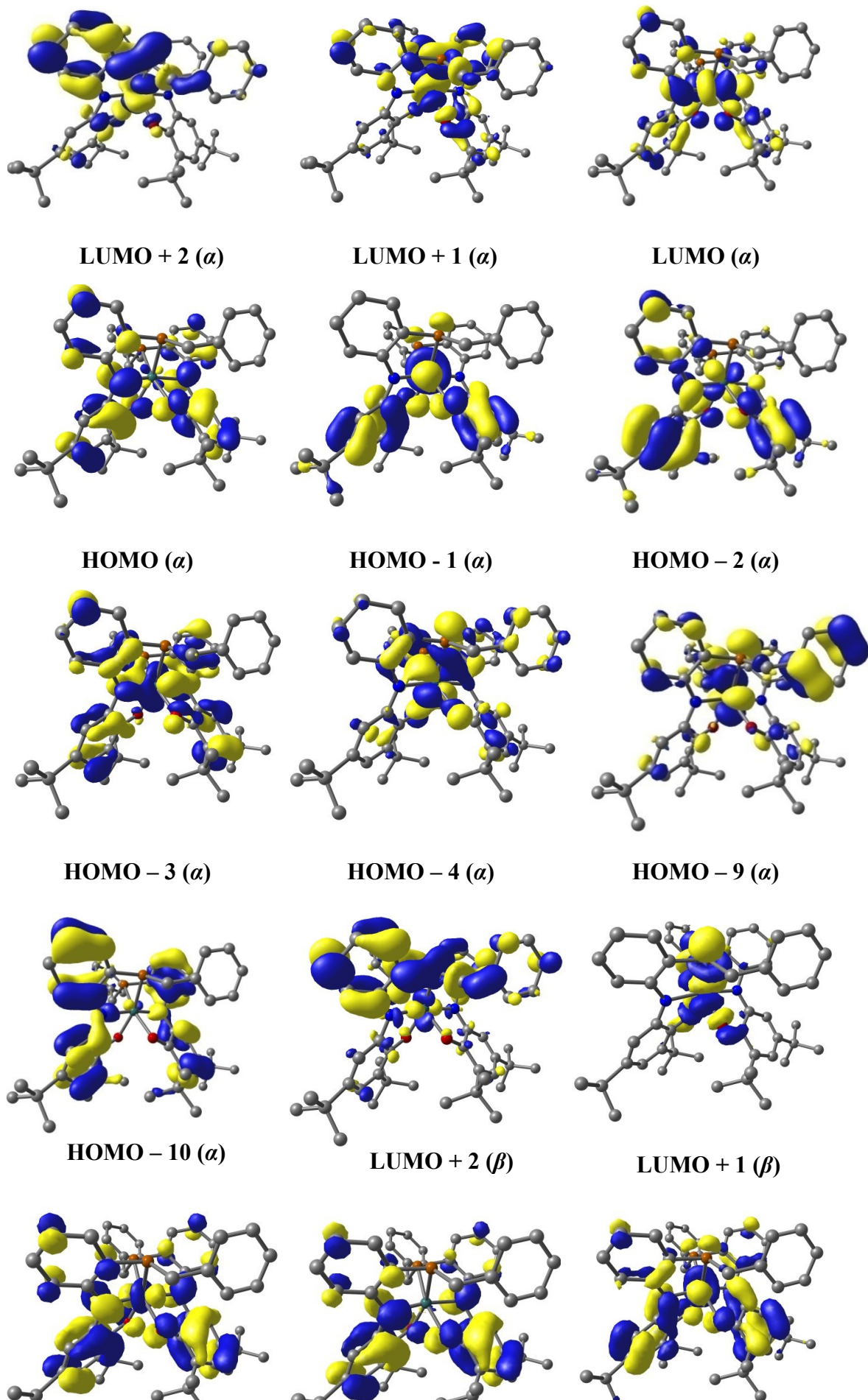
**Fig. S21** Representative molecular-orbitals involved in TD-DFT transitions of **1**, using CAM-B3LYP level of theory.

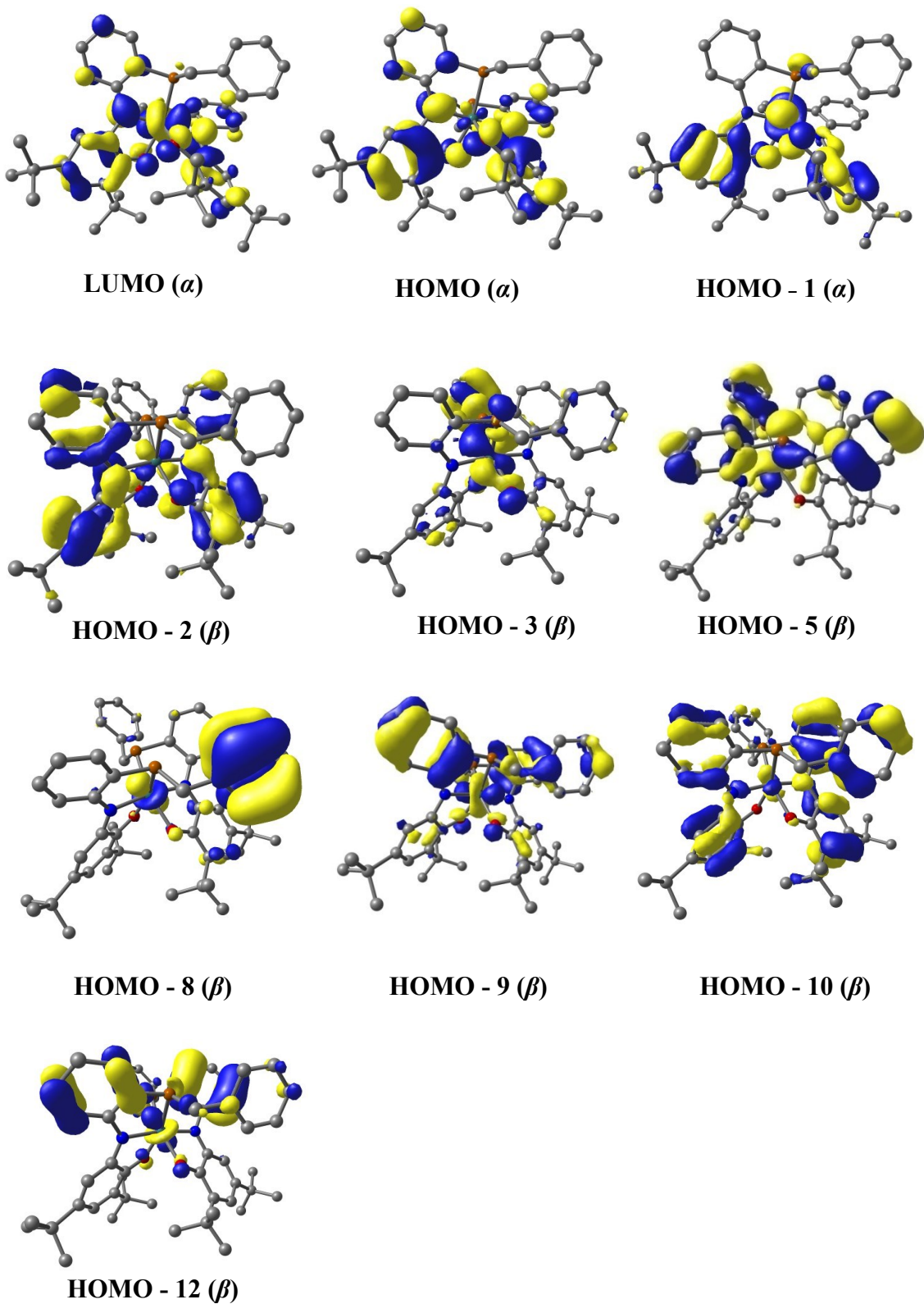




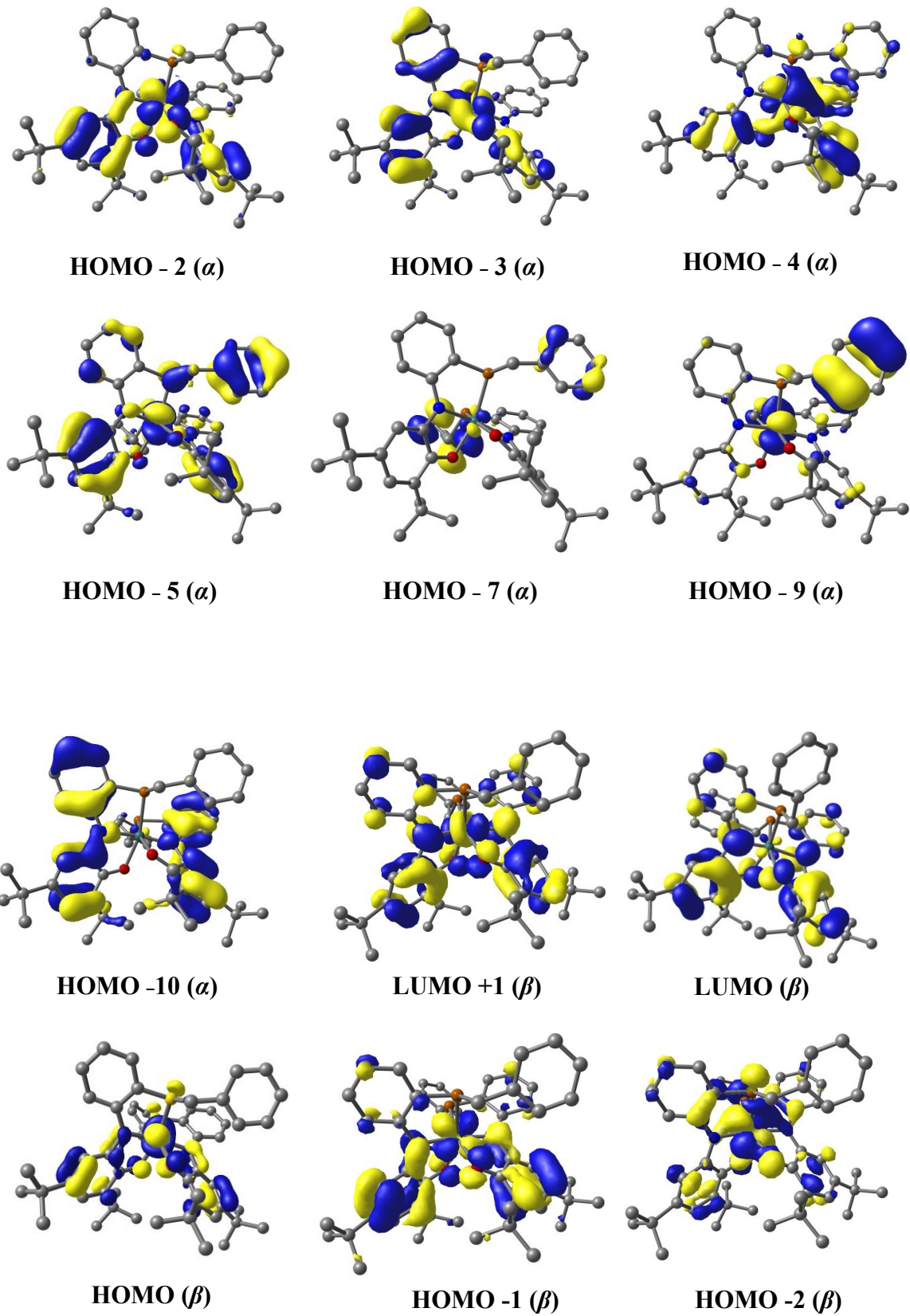


**Fig. S22** Representative molecular-orbitals involved in TD-DFT transitions of **1**, using B3LYP level of theory.





**Fig. S23** Representative molecular-orbitals involved in TD-DFT transitions of  $[1^{\text{Ox1}}]^{1+}$ , using CAM-B3LYP level of theory.



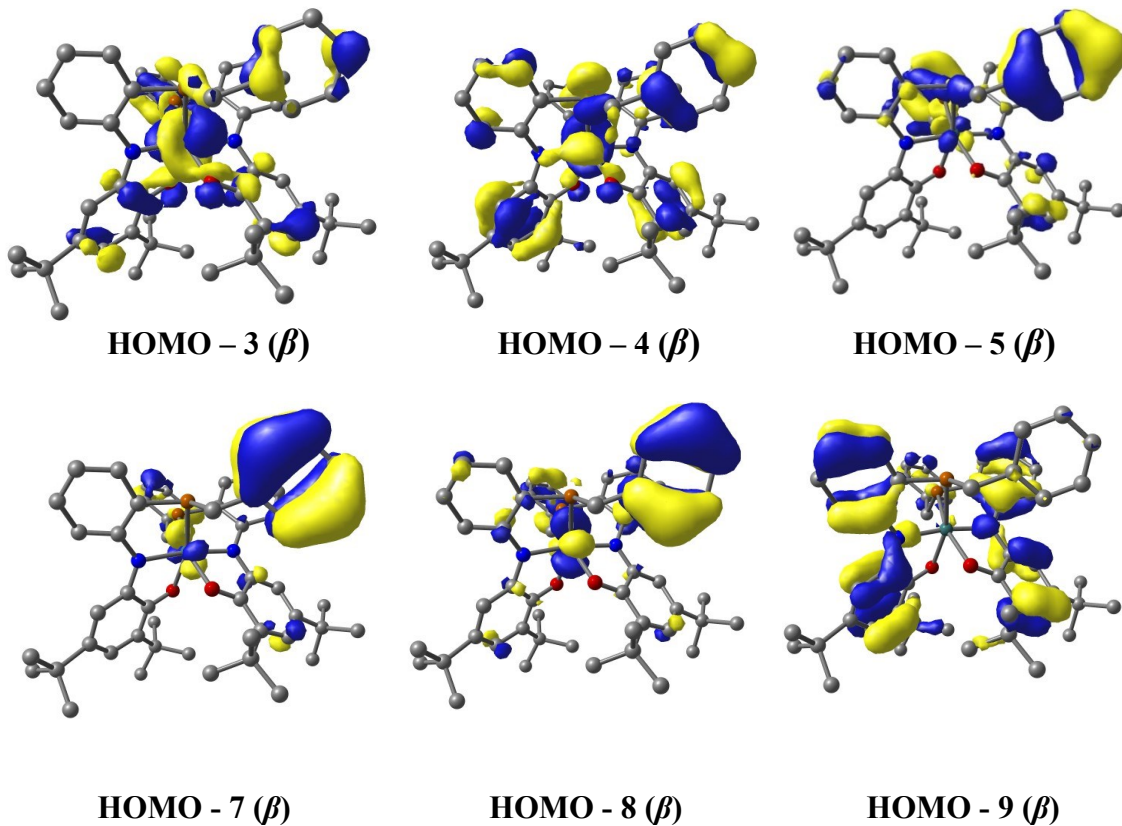


**Fig. S24** Representative molecular-orbitals involved in TD-DFT transitions of  $[1^{\text{Ox1}}]^{1+}$ , using B3LYP level of theory.

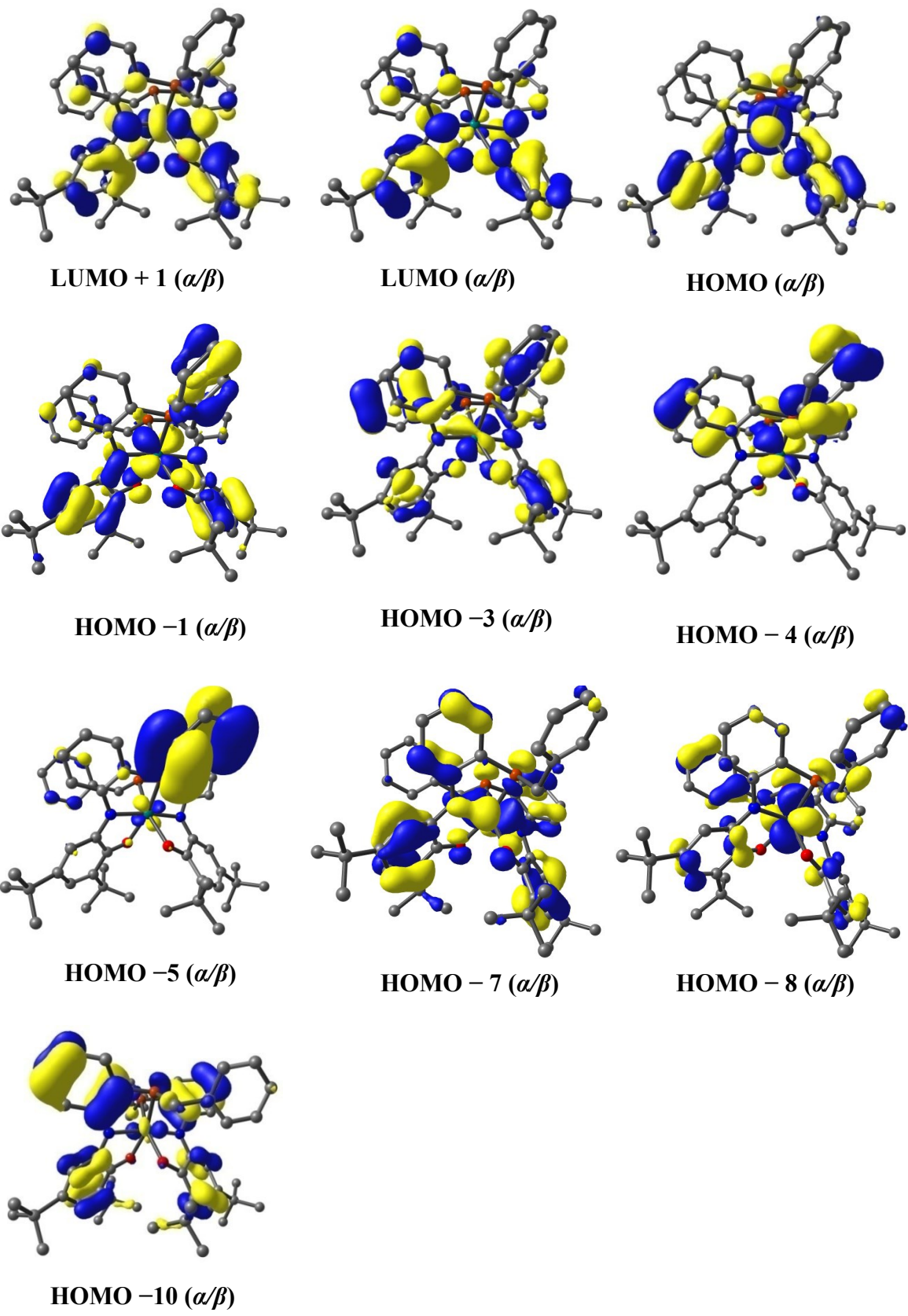


**Fig. S25** Representative molecular-orbitals involved in TD-DFT transitions of  $[1^{ox2}]^{2+}$ , using CAM-B3LYP level of theory.

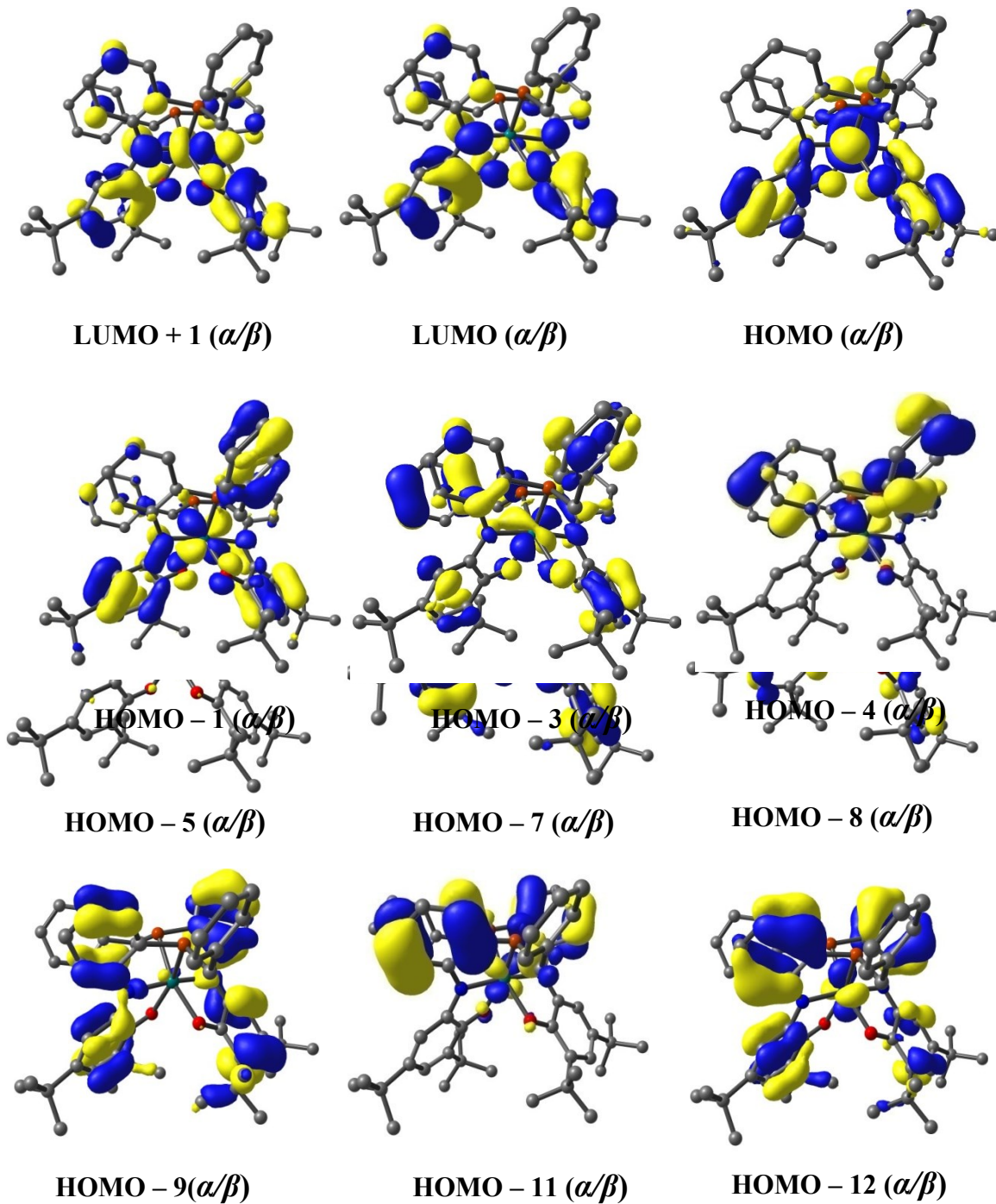


**Fig. S26** Representative molecular-orbitals involved in TD-DFT transitions of  $[1^{\text{ox2}}]^{2+}$ , using B3LYP level of theory.

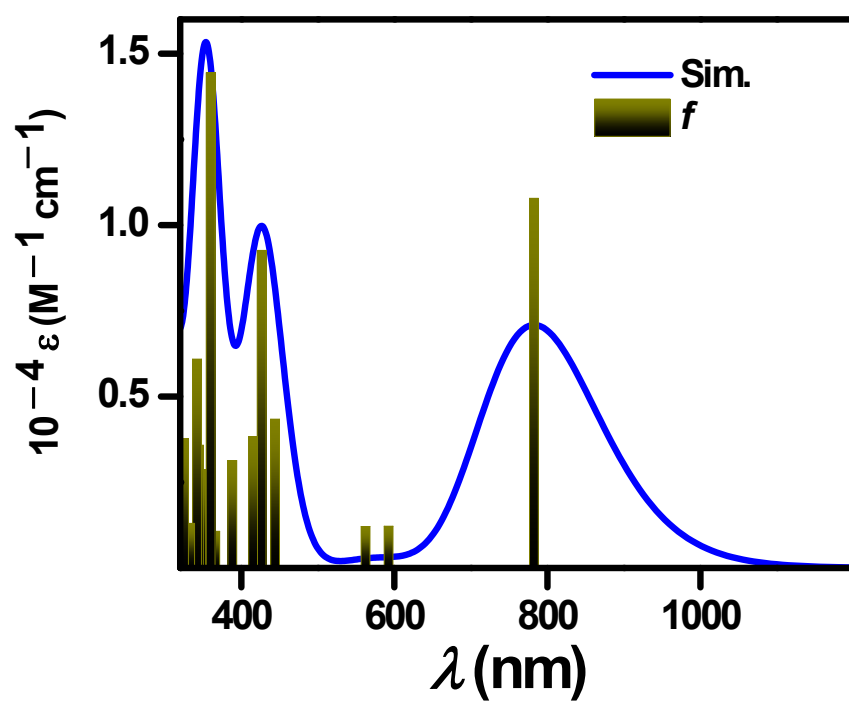


**Fig. S27** TD-DFT calculated spectra of free ligand in its ( $L^{ISQ}^{*-}$  redox level using CAM-B3LYP level of theory.

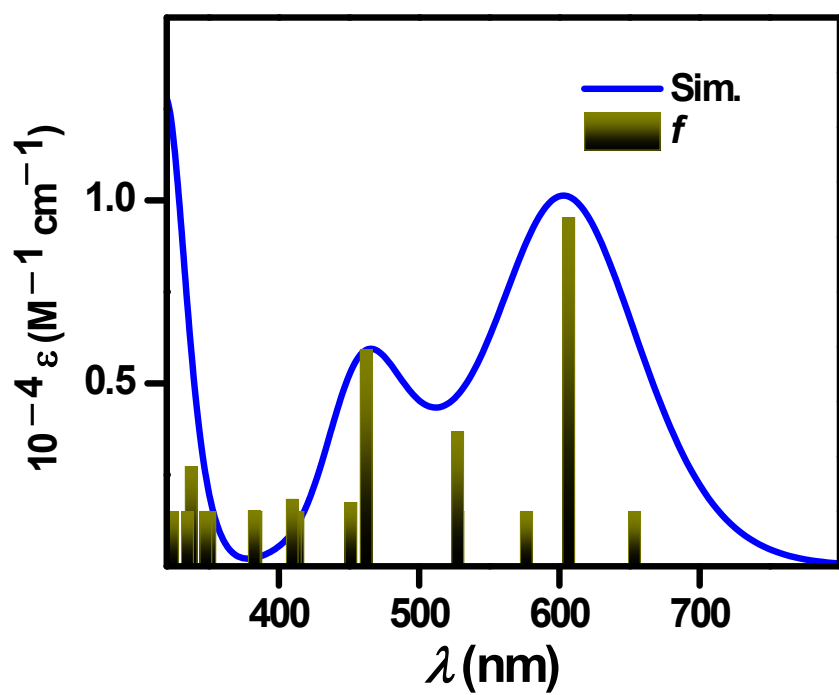


**Fig. S28** TD-DFT calculated spectra of free ligand in its  $(L^{IBQ})^0$  redox level using CAM-B3LYP level of theory.

**Table S1** Crystal data and structure refinement parameters for **1** at 100 K and at 298 K

	100 K	298 K
formula	C <sub>54</sub> H <sub>62</sub> N <sub>2</sub> O <sub>2</sub> RuS <sub>2</sub>	C <sub>54</sub> H <sub>62</sub> N <sub>2</sub> O <sub>2</sub> RuS <sub>2</sub>
fw	936.30	936.30
T/K	100(2)	298(2)
cryst color, habit	purple, block	purple, block
cryst syst	triclinic	triclinic
space group	P $\bar{1}$ (No. 2)	P $\bar{1}$ (No. 2)
a/Å	10.489(2);	10.568(5)
b/Å	11.622(2)	11.825(5)
c/Å	21.239(4)	21.385(5)
$\alpha$ /deg	82.011(3)	81.660(5)
$\beta$ /deg	84.971(4)	85.142(5)
$\gamma$ /deg	67.666 (4)	67.475(5)
V/Å <sup>3</sup>	2369.9(8)	2441.2(17)
Z	2	2
D <sub>c</sub> /g cm <sup>-3</sup>	1.312	1.274
F(000)	984	984
$\mu$ /mm <sup>-1</sup>	0.461	0.448
reflns collected	13298	36768
unique reflns/R <sub>int</sub>	9077/0.0359	36740/0.0716
reflns used [ $I > 2\sigma(I)$ ]	6907	7855
GOF on $F^2$	0.984	1.026
$R_1$ , <sup>a</sup> wR <sub>2</sub> <sup>b</sup> [ $I > 2\sigma(I)$ ]	$R_1 = 0.058$ wR <sub>2</sub> = 0.144	$R_1 = 0.0731$ wR <sub>2</sub> = 0.1579
$R_1$ , <sup>a</sup> wR <sub>2</sub> <sup>b</sup> (all data)	$R_1 = 0.081$ wR <sub>2</sub> = 0.179	$R_1 = 0.1289$ wR <sub>2</sub> = 0.1825

<sup>a</sup> $R_1 = \sum ||F_{\text{o}}| - |F_{\text{c}}|| / \sum |F_{\text{o}}|$ . <sup>b</sup>wR<sub>2</sub> = { $\sum [w(|F_{\text{o}}|^2 - |F_{\text{c}}|^2)^2] / \sum [w(|F_{\text{o}}|^2)^2]$ }<sup>1/2</sup>

**Table S2** Crystal data and structure refinement parameters for **2** and **3** at 100 K and at 298 K

formula	<b>2</b> $C_{55}H_{63}Cl_2F_6N_2O_3PRuS_2$		<b>3</b> $C_{54}H_{62}F_8N_2O_{3.7}B_2RuS_2$	
Fw	1183.19	1183.19	1140.95	1140.95
T/K	100(2)	298(2)	100(2)	298(2)
Cryst color, habit	bluish purple, block		dark green, block	
Cryst syst space group	Monoclinic $P2_1/c$ (No. 14)		Monoclinic $P2_1/c$ (No. 14)	
$a/\text{\AA}$	15.4686(3)	15.6743(2)	15.1356(3)	15.3134(5)
$b/\text{\AA}$	21.8136(3)	21.9974(2)	21.8710(3)	22.0442 (6)
$c/\text{\AA}$	17.1423(3)	17.5755(2)	16.8585(3)	17.0690(5)
$\alpha/\text{deg}$	90.000	90.000	90.000	90.000
$\beta/\text{deg}$	109.838(2)	110.007(2)	109.946(2)	110.040(3)
$\gamma/\text{deg}$	90.000	90.000	90.000	90.000
$V/\text{\AA}^3$	5440.99(17)	5694.21(13)	5245.92(17)	5413.1(3)
Z	4	4	4	4
$D_c/\text{g cm}^{-3}$	1.442	1.381	1.440	1.381
$F(000)$	2440	2451.6	2350.4	2328.0
$\mu/\text{mm}^{-1}$	4.78	4.57	3.80	3.67
reflns collected	37843	46101	49850	37983
unique reflns/ $R_{\text{int}}$	37248/0.0315	45440/0.0287	49031/0.0655	37375
reflns used [ $I > 2\sigma(I)$ ]	8884	8947	8587	8606
GOF on $F^2$	1.047	1.0510	1.0300	1.0500
$R_1,^a wR_2^b$ [ $I > 2\sigma(I)$ ]	$R_1 = 0.0658$ $wR_2 = 0.1890$	$R_1 = 0.0636$ $wR_2 = 0.2039$	$R_1 = 0.0831$ $wR_2 = 0.2272$	$R_1 = 0.0732$ $wR_2 = 0.2107$
$R_1,^a wR_2^b$ (all data)	$R_1 = 0.0686$ $wR_2 = 0.1934$	$R_1 = 0.0677$ $wR_2 = 0.2097$	$R_1 = 0.0861$ $wR_2 = 0.2307$	$R_1 = 0.0770$ $wR_2 = 0.2160$

<sup>a</sup>  $R_1 = \Sigma ||F_o| - |F_c|| / \Sigma |F_o|$ . <sup>b</sup>  $wR_2 = \{\Sigma [w(|F_o|^2 - |F_c|^2)^2] / \Sigma [w(|F_o|^2)^2]\}^{1/2}$

CCDC-1899166 (**1**; 298 K dataset), 1899167 (**1**; 100 K dataset), 1899168 (**2**; 100 K dataset), 1936878 (**2**; 298 K dataset), 1899169 (**3**; 100 K dataset), and 1936879 (**3**; 298K dataset).

**Table S3** Bond angles for **1**, **2** and **3** at 100 K and at 298 K

	<b>1</b>	<b>2</b>	<b>3</b>
N1–Ru–N2	168.10(13) [168.45(13)]	166.82(16) [167.39(14)]	166.93(19) [167.35(16)]
N1–Ru–O2	90.37(12) [90.55(13)]	90.01(14) [91.15(13)]	89.32(17) [89.87(15)]
N1–Ru–O1	81.15(12) [80.98(12)]	80.04(15) [79.87(13)]	79.91(16) [79.99(14)]
N2–Ru–O1	90.00(12) [90.73(13)]	90.79(14) [90.65(14)]	92.06(17) [92.33 (16)]
N2–Ru–O2	81.24(12) [81.07(13)]	80.06(14) [80.02(14)]	79.75(18) [79.57(16)]
O1–Ru–O2	87.32(11) [87.92(12)]	87.43(13) [87.21(13)]	85.82(16) [86.48(14)]
N1–Ru–S2	105.05(10) [104.94(11)]	105.29(11) [104.30(11)]	106.01(13) [105.96(12)]
N1–Ru–S1	83.83(9) [83.73(10)]	85.09(12) [84.58(10)]	85.17(14) [84.87(12)]
N2–Ru–S1	105.33(10) [104.94(10)]	104.53(11) [104.98(10)]	103.12(14) [103.10(13)]
N2–Ru–S2	83.85(10) [83.92(10)]	84.77(11) [84.91(11)]	84.92(14) [84.67(12)]
S1–Ru–S2	83.43(4) [83.49(4)]	85.20(4) [85.49(4)]	85.61(5) [85.49(4)]
O1–Ru–S1	164.63(8) [164.25(8)]	164.61(9) [164.36(9)]	164.82(11) [164.57(11)]
O1–Ru–S2	97.30(8) [96.81(9)]	94.85(10) [96.65(9)]	95.76(11) [95.76(10)]
O2–Ru–S1	96.05(8) [ 96.00(9)]	96.58(10) [94.85(9)]	96.86(12) [95.76(10)]
O2–Ru–S2	164.39(8) [164.32(8)]	164.69(9) [164.49(9)]	164.64(12) [164.57(10)]

<sup>a</sup> The values in parentheses are at 298 K.

**Table S4** Comparison of experimental bond lengths (X-ray) with calculated bond lengths (MOS values) (Å) of **1**, **2** and **3** at 298 K

Bond distances (Å)	<b>1</b>	MOS-derived parameters of <b>1</b>	<b>2</b>	MOS-derived parameters of <b>2</b>	<b>3</b>	MOS-derived parameters of <b>3</b>
C1–O1	1.333(4)	1.337	1.302(6)	1.302	1.302(6)	1.302
C1–C2	1.411(5)	1.410	1.364(6)	1.349	1.364(6)	1.349
C2–C7	1.390(5)	1.392	1.424(6)	1.426	1.424(6)	1.426
C7–C8	1.413(5)	1.406	1.374(7)	1.377	1.374(7)	1.377
C8–C13	1.380(5)	1.384	1.432(6)	1.428	1.432(6)	1.428
C13–C14	1.389(5)	1.400	1.373(7)	1.371	1.373(7)	1.371
C1–C14	1.433(5)	1.421	1.411(6)	1.412	1.411(6)	1.412
C14–N1	1.394(5)	1.378	1.454(6)	1.443	1.454(6)	1.443
C28–O2	1.329(5)	1.322	1.302(6)	1.302	1.302(6)	1.302
C28–C29	1.410(6)	1.416	1.364(6)	1.349	1.364(6)	1.349
C29–C34	1.370(6)	1.386	1.424(6)	1.426	1.424(6)	1.426
C34–C35	1.433(5)	1.416	1.374(7)	1.377	1.374(7)	1.377
C40–C41	1.403(5)	1.405	1.432(6)	1.428	1.432(6)	1.428
C28–C41	1.434(5)	1.429	1.373(7)	1.371	1.373(7)	1.371
C35–C40	1.360(6)	1.379	1.411(6)	1.412	1.411(6)	1.412
C41–N2	1.387(5)	1.366	1.454(6)	1.443	1.454(6)	1.443

**Table S5** DFT-optimized cartesian coordinates of **1**, using CAM-B3LYP**RuC54S2O2N2H62**

Ru	-0.030859000	0.021899000	-0.065508000
S	-0.155944000	-0.130295000	2.331001000
S	2.363502000	0.123803000	0.181467000
O	-1.949489000	-0.636165000	-0.406506000
O	-0.069062000	0.734165000	-2.000430000
N	-0.645994000	1.923723000	0.252674000
N	0.339392000	-1.870712000	-0.644872000
C	-0.825627000	1.790821000	-2.085874000
C	-1.944408000	-1.689145000	-1.180758000
C	-0.703026000	-2.397058000	-1.362593000

C	-1.194489000	2.472462000	-0.870289000
C	-1.808795000	-0.779821000	2.841078000
C	-0.354806000	1.632287000	2.607712000
C	3.127099000	0.761673000	-1.375824000
C	2.623552000	-1.645308000	0.021721000
C	-0.561909000	2.498634000	1.509521000
C	1.548223000	-2.480773000	-0.360554000
C	-1.258611000	2.320082000	-3.342410000
C	-3.124839000	-2.183476000	-1.806940000
C	-0.642452000	-3.488938000	-2.248915000
C	-2.087104000	3.568658000	-0.918944000
C	-1.715925000	-2.253511000	3.119918000
C	-0.227596000	2.130081000	3.899313000
C	3.448073000	2.222240000	-1.230582000
C	3.863950000	-2.178166000	0.352806000
C	-0.578423000	3.880957000	1.768119000
C	1.767492000	-3.870076000	-0.337978000
C	-0.830549000	1.660120000	-4.661088000
C	-2.096376000	3.414927000	-3.310223000
C	-2.994806000	-3.285380000	-2.636406000
C	-4.477525000	-1.488571000	-1.590529000
C	-1.773057000	-3.942594000	-2.897197000
C	-2.552063000	4.042557000	-2.121986000
C	-2.002105000	-3.186656000	2.123195000
C	-1.318146000	-2.709256000	4.378246000
C	-0.298584000	3.496707000	4.138027000
C	4.670213000	2.625188000	-0.689311000
C	2.525127000	3.196315000	-1.612679000
C	4.072760000	-3.551043000	0.317242000
C	-0.455984000	4.364461000	3.060913000
C	3.010268000	-4.388612000	-0.011561000
C	-1.350938000	0.211781000	-4.722439000
C	-1.381862000	2.407871000	-5.882560000
C	0.704935000	1.655806000	-4.774781000
C	-4.415057000	-0.036236000	-2.098854000
C	-5.615233000	-2.196517000	-2.338666000
C	-4.836892000	-1.489692000	-0.093154000
C	-1.665683000	-5.116827000	-3.880741000
C	-3.547354000	5.202429000	-2.229526000
C	-1.893888000	-4.548937000	2.382116000
C	-1.209551000	-4.069330000	4.637755000
C	4.966934000	3.973154000	-0.534068000
C	2.821399000	4.546362000	-1.458087000
C	-1.092370000	-6.348231000	-3.155963000
C	-3.023151000	-5.510228000	-4.476541000
C	-0.729545000	-4.730640000	-5.040308000

C	-2.915998000	6.349130000	-3.040098000
C	-3.946202000	5.753879000	-0.855958000
C	-4.825441000	4.719756000	-2.939859000
C	-1.496528000	-4.993424000	3.637825000
C	4.040933000	4.938052000	-0.917952000
H	-2.454626000	3.812605000	-4.250532000
H	-2.435813000	3.992403000	0.011306000
H	-0.646807000	4.573594000	0.940083000
H	-0.465471000	5.437002000	3.227150000
H	-0.200085000	3.880584000	5.147378000
H	-0.052754000	1.438472000	4.718122000
H	-4.433802000	4.993552000	-0.239147000
H	-4.651815000	6.580073000	-0.981334000
H	-3.082061000	6.139047000	-0.306489000
H	-2.013854000	6.723956000	-2.547607000
H	-3.621368000	7.180849000	-3.136499000
H	-2.638180000	6.031750000	-4.048215000
H	-5.294935000	3.903870000	-2.382884000
H	-4.617912000	4.357020000	-3.949531000
H	-5.548399000	5.537924000	-3.022148000
H	-5.741845000	-3.232843000	-2.010852000
H	-5.458860000	-2.194092000	-3.421340000
H	-6.554664000	-1.671889000	-2.142705000
H	-3.630659000	0.527244000	-1.593709000
H	-5.374325000	0.462318000	-1.920628000
H	-4.219888000	-0.012129000	-3.174787000
H	-4.096591000	-0.934080000	0.481737000
H	-4.891489000	-2.511267000	0.296634000
H	-5.814501000	-1.020131000	0.057988000
H	-2.475671000	2.410958000	-5.904243000
H	-1.038439000	1.909373000	-6.793299000
H	-1.032699000	3.444286000	-5.922310000
H	-3.734587000	-5.815104000	-3.703538000
H	-2.893143000	-6.356247000	-5.157563000
H	-3.469414000	-4.692391000	-5.049247000
H	-1.114310000	-3.858325000	-5.576243000
H	-0.640030000	-5.557523000	-5.752639000
H	0.274448000	-4.485845000	-4.684476000
H	-0.095761000	-6.153068000	-2.751239000
H	-1.009428000	-7.194869000	-3.845317000
H	-1.738474000	-6.648618000	-2.325721000
H	-0.981908000	-0.379848000	-3.884747000
H	-1.023375000	-0.260688000	-5.654931000
H	-2.444278000	0.193584000	-4.703043000
H	1.150028000	1.075299000	-3.967492000
H	1.104832000	2.674200000	-4.738695000

H	1.007066000	1.209273000	-5.727695000
H	-3.880595000	-3.652080000	-3.132776000
H	0.319011000	-3.942157000	-2.452622000
H	0.941315000	-4.539337000	-0.536977000
H	3.145787000	-5.465435000	0.004204000
H	5.042322000	-3.962952000	0.574426000
H	4.662782000	-1.508923000	0.658299000
H	4.031632000	0.170258000	-1.529386000
H	2.417513000	0.571177000	-2.180413000
H	5.397045000	1.873908000	-0.391627000
H	5.923636000	4.271111000	-0.116937000
H	4.272461000	5.991899000	-0.800240000
H	2.095957000	5.292823000	-1.765827000
H	1.574019000	2.893485000	-2.035557000
H	-2.084086000	-0.222859000	3.738795000
H	-2.505825000	-0.552952000	2.034792000
H	-1.095603000	-1.989896000	5.162076000
H	-0.904285000	-4.408683000	5.622498000
H	-1.414644000	-6.056721000	3.839758000
H	-2.124846000	-5.263023000	1.597970000
H	-2.312372000	-2.842868000	1.143155000

**Table S6** DFT-optimized cartesian coordinates of [1<sup>OX1</sup>]<sup>1+</sup>, using CAM-B3LYP**RuC54S2O2N2H62**

Ru	0.070038000	0.051519000	-0.085989000
S	0.070730000	-0.001825000	2.312572000
S	2.466506000	0.035855000	0.022149000
O	-0.091733000	0.690570000	-2.037400000
O	-1.895293000	-0.534409000	-0.268209000
N	0.288515000	-1.878905000	-0.613580000
N	-0.307834000	2.007423000	0.182103000
C	-2.006768000	-1.603743000	-0.976239000
C	-0.881137000	2.587361000	-0.890391000
C	-0.795942000	-2.369330000	-1.245099000
C	-0.717749000	1.814743000	-2.114535000
C	-1.667688000	-0.339408000	2.843718000
C	0.205988000	1.773090000	2.514829000
C	2.638042000	-1.741676000	-0.140990000
C	3.202182000	0.666108000	-1.551507000
C	1.507542000	-2.537874000	-0.412342000
C	0.011514000	2.617987000	1.401603000
C	-3.272376000	-2.090937000	-1.453372000

C	-1.595302000	3.814508000	-0.915780000
C	-0.847263000	-3.494055000	-2.111561000
C	-1.189396000	2.352340000	-3.360480000
C	-1.870291000	-0.131305000	4.314876000
C	0.572701000	2.290372000	3.750999000
C	3.878454000	-2.322448000	0.099069000
C	3.472655000	2.139924000	-1.426227000
C	1.655962000	-3.931143000	-0.368480000
C	0.254079000	3.987716000	1.561428000
C	-4.578513000	-1.371839000	-1.096570000
C	-3.234808000	-3.205793000	-2.248037000
C	-2.082257000	4.302104000	-2.096205000
C	-2.042600000	-3.909214000	-2.627219000
C	-1.837896000	3.558481000	-3.297833000
C	-1.004596000	1.580531000	-4.674091000
C	-1.377674000	-1.056108000	5.238996000
C	-2.547604000	0.996179000	4.778209000
C	0.759031000	3.659894000	3.901779000
C	4.018552000	-3.704012000	0.079231000
C	2.659522000	3.068016000	-2.075531000
C	4.540890000	2.598489000	-0.651898000
C	2.898430000	-4.500994000	-0.134710000
C	0.615231000	4.497010000	2.801022000
C	-4.753779000	-1.354289000	0.433565000
C	-5.798683000	-2.079945000	-1.699406000
C	-4.557267000	0.071184000	-1.634965000
C	-2.890375000	5.596998000	-2.192383000
C	-2.167102000	-5.085404000	-3.596651000
C	-1.575458000	2.353507000	-5.870077000
C	-1.737817000	0.228231000	-4.593266000
C	0.492128000	1.338560000	-4.944176000
C	-1.557075000	-0.854014000	6.600680000
C	-2.731130000	1.197628000	6.142164000
C	2.909277000	4.431371000	-1.953911000
C	4.789473000	3.958834000	-0.527823000
C	-4.282515000	5.288656000	-2.774960000
C	-2.153410000	6.585777000	-3.115581000
C	-3.079081000	6.263838000	-0.825393000
C	-3.070244000	-6.165039000	-2.970390000
C	-2.791398000	-4.593903000	-4.916319000
C	-0.808182000	-5.719238000	-3.913205000
C	-2.233827000	0.275078000	7.054666000
C	3.971872000	4.878957000	-1.177931000
H	4.171223000	5.941653000	-1.087352000
H	2.276609000	5.142634000	-2.475113000
H	5.627355000	4.301885000	0.069895000

H	0.805997000	5.560175000	2.900985000
H	1.042313000	4.064467000	4.866828000
H	0.720820000	1.617828000	4.588513000
H	-2.941556000	1.715763000	4.066314000
H	-3.266102000	2.074736000	6.490869000
H	-2.378461000	0.430058000	8.118676000
H	-1.175545000	-1.581249000	7.309663000
H	-0.854536000	-1.941621000	4.887755000
H	2.988298000	-5.581465000	-0.102267000
H	4.987317000	-4.154405000	0.263180000
H	0.787580000	-4.566465000	-0.481011000
H	-3.789490000	-4.173829000	-4.770015000
H	-2.167771000	-3.826349000	-5.383500000
H	-2.885191000	-5.427525000	-5.617994000
H	-3.172892000	-7.009297000	-3.657924000
H	-0.946591000	-6.553980000	-4.604562000
H	-0.126869000	-5.008481000	-4.389809000
H	-0.324453000	-6.116091000	-3.015656000
H	0.076291000	-3.976938000	-2.393419000
H	-4.168622000	-3.579992000	-2.644525000
H	4.731761000	-1.689611000	0.322294000
H	4.124147000	0.096522000	-1.686854000
H	2.509892000	0.436820000	-2.361072000
H	5.186674000	1.884515000	-0.147693000
H	1.837510000	2.720593000	-2.691230000
H	-5.491443000	0.575808000	-1.370328000
H	-3.727683000	0.643886000	-1.219677000
H	-4.472278000	0.076186000	-2.725404000
H	-5.898916000	-3.107565000	-1.337957000
H	-5.767737000	-2.096956000	-2.792803000
H	-6.704236000	-1.542026000	-1.408397000
H	-4.783156000	-2.371776000	0.835210000
H	-3.942869000	-0.810592000	0.917544000
H	-5.697054000	-0.865123000	0.693508000
H	-4.225434000	4.853404000	-3.775694000
H	-4.868189000	6.209226000	-2.850473000
H	-4.829698000	4.590884000	-2.134728000
H	-1.163668000	6.830510000	-2.719209000
H	-2.723282000	7.515553000	-3.198145000
H	-2.023110000	6.190404000	-4.125992000
H	-2.221968000	3.978610000	-4.217254000
H	-2.652745000	2.519264000	-5.778186000
H	-1.085238000	3.321910000	-6.007359000
H	-1.412900000	1.773351000	-6.781673000
H	-1.349935000	-0.391923000	-3.784680000
H	-1.610447000	-0.315627000	-5.534329000

H	-2.809708000	0.377370000	-4.435555000
H	0.614177000	0.805941000	-5.891811000
H	1.035993000	2.284946000	-5.023982000
H	0.943835000	0.735804000	-4.155990000
H	0.207535000	4.644258000	0.702940000
H	-3.626370000	5.620896000	-0.129940000
H	-2.123192000	6.536055000	-0.367843000
H	-3.657094000	7.183483000	-0.944165000
H	-1.822370000	-1.379406000	2.546866000
H	-2.321880000	0.285447000	2.236404000
H	-1.788768000	4.322544000	0.017211000
H	-2.644666000	-6.540322000	-2.035327000
H	-4.075128000	-5.792464000	-2.756947000

**Table S7** DFT-optimized cartesian coordinates of  $[1\text{O}x^2]^{2+}$ , using CAM-B3LYP**RuC54S2O2N2H62**

Ru	0.051804000	0.043588000	-0.145400000
S	0.023346000	-0.057219000	2.225945000
S	2.416209000	0.056798000	-0.037744000
O	-0.166590000	0.745548000	-2.118493000
O	-1.949192000	-0.587505000	-0.386801000
N	0.253710000	-1.926565000	-0.653621000
N	-0.270962000	2.042873000	0.121790000
C	-2.054030000	-1.678351000	-0.992709000
C	-0.782638000	2.673894000	-0.909805000
C	-0.796742000	-2.459530000	-1.237444000
C	-0.682000000	1.885037000	-2.182076000
C	-1.713148000	-0.409240000	2.774919000
C	0.167590000	1.711814000	2.472550000
C	2.628297000	-1.710001000	-0.260651000
C	3.188769000	0.782776000	-1.549883000
C	1.516131000	-2.543854000	-0.490991000
C	0.028884000	2.600125000	1.385528000
C	-3.329216000	-2.236621000	-1.406856000
C	-1.410127000	3.963224000	-0.929163000
C	-0.848352000	-3.635547000	-2.056849000
C	-1.122419000	2.480457000	-3.430406000
C	-1.893750000	-0.215874000	4.250059000
C	0.506685000	2.185760000	3.732119000
C	3.891105000	-2.257925000	-0.074963000
C	3.288591000	2.275961000	-1.384384000
C	1.695542000	-3.931579000	-0.427564000

C	0.331131000	3.952478000	1.580550000
C	-4.647302000	-1.530221000	-1.071603000
C	-3.261796000	-3.392154000	-2.117384000
C	-1.849689000	4.484037000	-2.100458000
C	-2.041846000	-4.091242000	-2.509365000
C	-1.652735000	3.727156000	-3.332756000
C	-1.022643000	1.707303000	-4.751424000
C	-1.358928000	-1.133657000	5.158163000
C	-2.595750000	0.889917000	4.730013000
C	0.736104000	3.545729000	3.923672000
C	4.064818000	-3.637590000	-0.090910000
C	2.585462000	3.127189000	-2.236554000
C	4.098712000	2.828403000	-0.388777000
C	2.960393000	-4.468901000	-0.238665000
C	0.672125000	4.417215000	2.843486000
C	-4.794680000	-1.406036000	0.456683000
C	-5.850984000	-2.320582000	-1.600301000
C	-4.676429000	-0.131559000	-1.717846000
C	-2.570587000	5.823462000	-2.202579000
C	-2.183715000	-5.301123000	-3.425849000
C	-1.562545000	2.538149000	-5.922534000
C	-1.860771000	0.416766000	-4.660494000
C	0.444723000	1.353395000	-5.058429000
C	-1.521370000	-0.944298000	6.523743000
C	-2.763447000	1.076305000	6.098080000
C	2.686107000	4.508213000	-2.095795000
C	4.196455000	4.206454000	-0.245395000
C	-3.968850000	5.602042000	-2.813682000
C	-1.748632000	6.760124000	-3.111431000
C	-2.737653000	6.493169000	-0.834877000
C	-3.039161000	-6.367976000	-2.711993000
C	-2.879034000	-4.866102000	-4.731618000
C	-0.826772000	-5.918883000	-3.777494000
C	-2.223539000	0.162264000	6.995287000
C	3.487775000	5.049621000	-1.096933000
H	3.578916000	6.125849000	-0.994774000
H	2.153352000	5.160664000	-2.780106000
H	4.839854000	4.623735000	0.521773000
H	0.910418000	5.466517000	2.977332000
H	1.001750000	3.913084000	4.908593000
H	0.608013000	1.490034000	4.557272000
H	-3.026722000	1.601060000	4.030709000
H	-3.320729000	1.932623000	6.462454000
H	-2.356473000	0.305216000	8.062280000
H	-1.109379000	-1.664654000	7.222214000
H	-0.818906000	-2.004085000	4.794603000

H	3.079535000	-5.545391000	-0.188127000
H	5.052720000	-4.059384000	0.056194000
H	0.841147000	-4.592678000	-0.478912000
H	-3.879353000	-4.460428000	-4.560984000
H	-2.290254000	-4.112298000	-5.261768000
H	-2.988879000	-5.730864000	-5.390604000
H	-3.150083000	-7.238702000	-3.362914000
H	-0.978865000	-6.778872000	-4.432864000
H	-0.180769000	-5.215000000	-4.310433000
H	-0.298748000	-6.279312000	-2.889568000
H	0.075785000	-4.103834000	-2.358201000
H	-4.189253000	-3.830660000	-2.458886000
H	4.738769000	-1.607019000	0.113866000
H	4.174016000	0.315947000	-1.622646000
H	2.594180000	0.498510000	-2.418121000
H	4.666863000	2.178854000	0.271361000
H	1.984330000	2.707631000	-3.036523000
H	-5.629066000	0.353838000	-1.489739000
H	-3.874234000	0.506384000	-1.343928000
H	-4.591875000	-0.203093000	-2.805970000
H	-5.912895000	-3.321008000	-1.162269000
H	-5.839378000	-2.414261000	-2.690135000
H	-6.769078000	-1.793667000	-1.332154000
H	-4.770868000	-2.388827000	0.936723000
H	-4.009545000	-0.785085000	0.888330000
H	-5.756466000	-0.945039000	0.695524000
H	-3.927481000	5.174139000	-3.818459000
H	-4.487721000	6.560511000	-2.892575000
H	-4.574849000	4.942428000	-2.186389000
H	-0.753573000	6.942618000	-2.695901000
H	-2.257999000	7.723115000	-3.197417000
H	-1.628581000	6.366989000	-4.124084000
H	-1.999192000	4.201627000	-4.240611000
H	-2.621085000	2.785980000	-5.801258000
H	-0.999372000	3.464868000	-6.066046000
H	-1.470212000	1.959162000	-6.843800000
H	-1.484178000	-0.259053000	-3.891120000
H	-1.822698000	-0.108008000	-5.618753000
H	-2.908716000	0.645469000	-4.446775000
H	0.497666000	0.809672000	-6.005251000
H	1.054194000	2.255492000	-5.166595000
H	0.880383000	0.719325000	-4.284789000
H	0.362252000	4.629269000	0.737570000
H	-3.338680000	5.885735000	-0.151816000
H	-1.774065000	6.705760000	-0.362054000
H	-3.253563000	7.447492000	-0.958421000

H	-1.860003000	-1.448967000	2.471823000
H	-2.379653000	0.220707000	2.186303000
H	-1.588638000	4.470443000	0.006183000
H	-2.566296000	-6.700183000	-1.783768000
H	-4.044885000	-6.013187000	-2.473480000

**Table S8** X-ray determined and calculated [CAM-B3LYP (BS-DFT) and B3LYP (DFT)] bond lengths ( $\text{\AA}$ ) of **1**

Bonds	<b>1</b> X-ray ( $\text{\AA}$ )	Calcd. param. using CAM- B3LYP (BS, $S = 0$ ) ( $\text{\AA}$ )	Calcd. param. using B3LYP (CSS, $S = 0$ ) QROs ( $\text{\AA}$ )
Ru1–N1	1.968(3)	2.024	1.983
Ru1–N2	1.964(3)	2.013	1.983
Ru1–O1	2.018(3)	2.062	2.029
Ru1–O2	2.015(3)	2.056	2.024
Ru1–S1	2.328(11)	2.404	2.349
Ru1–S2	2.328(11)	2.409	2.358
C14–N1	1.394(5)	1.365	1.377
C1–O1	1.333(4)	1.302	1.318
C1–C2	1.411(5)	1.430	1.403
C2–C7	1.390(5)	1.378	1.390
C7–C8	1.413(5)	1.418	1.407
C8–C13	1.380(5)	1.374	1.390
C13–C14	1.389(5)	1.414	1.404
C1–C14	1.433(5)	1.441	1.437
C41–N2	1.387(5)	1.370	1.378
C28–O2	1.329(5)	1.307	1.312
C28–C29	1.410(6)	1.424	1.405
C29–C34	1.370(6)	1.385	1.388
C34–C35	1.433(5)	1.411	1.408
C40–C41	1.403(5)	1.407	1.404
C28–C41	1.434(5)	1.440	1.434
C35–C40	1.360(6)	1.379	1.390

**Table S9** X-ray determined and calculated [CAM-B3LYP (BS-DFT) and B3LYP (DFT)] bond lengths ( $\text{\AA}$ ) of **2**

	<b>2</b> X-ray ( $\text{\AA}$ )	Calcd. param. using CAM-B3LYP (BS, $S = 1/2$ ) ( $\text{\AA}$ )	Calcd. param. using B3LYP ( $S = 1/2$ ) QROs ( $\text{\AA}$ )
Ru1–N1	1.991(4)	2.010	1.998
Ru1–N2	1.983(4)	2.013	1.996
Ru1–O1	2.022(3)	2.059	2.049
Ru1–O2	2.026(4)	2.058	2.048
Ru1–S1	2.325(11)	2.399	2.333
Ru1–S2	2.323(11)	2.398	2.331
C14–N1	1.355(6)	1.347	1.353
C1–O1	1.303(6)	1.289	1.294
C1–C2	1.421(7)	1.436	1.412
C2–C7	1.371(7)	1.370	1.379
C7–C8	1.432(7)	1.434	1.422
C8–C13	1.355(7)	1.370	1.377
C13–C14	1.425(7)	1.436	1.416
C1–C14	1.446(7)	1.456	1.454
C41–N2	1.364(6)	1.347	1.353
C28–O2	1.302(6)	1.287	1.292
C28–C29	1.424(6)	1.437	1.413
C29–C34	1.374(7)	1.369	1.377
C34–C35	1.432(6)	1.435	1.423
C40–C41	1.411(6)	1.420	1.413
C28–C41	1.454(6)	1.457	1.453
C35–C40	1.373(7)	1.366	1.377

**Table S10** X-ray determined and calculated [CAM-B3LYP (BS-DFT) and B3LYP(DFT)] bond lengths (Å) of **3**

	<b>3</b> X-ray (Å)	Calcd. param. using BS-DFT (Å)	Calcd. param. using B3LYP QROs (Å)
Ru1–N1	1.987(5)	2.042	2.014
Ru1–N2	1.994(5)	2.044	2.011
Ru1–O1	2.034(4)	2.105	2.071
Ru1–O2	2.038(4)	2.112	2.072
Ru1–S1	2.3198(14)	2.373	2.324
Ru1–S2	2.3125(13)	2.366	2.323
C14–N1	1.360(6)	1.313	1.332
C1–O1	1.296(7)	1.252	1.270
C1–C2	1.423(8)	1.451	1.421
C2–C7	1.368(8)	1.358	1.369
C7–C8	1.437(8)	1.459	1.438
C8–C13	1.379(8)	1.355	1.367
C13–C14	1.412(8)	1.434	1.429
C1–C14	1.459(8)	1.500	1.478
C41–N2	1.351(8)	1.314	1.332
C28–O2	1.297(7)	1.252	1.270
C28–C29	1.434(9)	1.452	1.422
C29–C34	1.362(9)	1.358	1.368
C34–C35	1.453(9)	1.450	1.439
C40–C41	1.413(8)	1.434	1.428
C28–C41	1.458(8)	1.500	1.476
C35–C40	1.349(9)	1.355	1.367

**Table S11** Mulliken spin densities for **1** and  $[1^{ox1}]^{1+}$ , using CAM-B3LYP and B3LYP functionals<sup>a</sup>

Complex	Density functional	Mulliken spin-densities			$\langle S^2 \rangle$
		Ru	(L) <sub>1</sub>	(L) <sub>2</sub>	
<b>1</b>	CAM-B3LYP	0.05	0.73	-0.78	0.7959
	B3LYP	0.02	-0.29	0.26	0.1437
$[1^{ox1}]^{1+}$	CAM-B3LYP	-0.49	0.74	0.76	1.0570
	B3LYP	-0.25	0.64	0.61	0.8297

<sup>a</sup> (L)<sub>1</sub> and (L)<sub>2</sub> represent two ligands.

**Table S12** Computed energy values of CSS and BS solution for **1**, using CAM-B3LYP and B3LYP functional

Density functional	$-E_{CSS}$ (a.u.)	$-E_{BS}$ (a.u.)
CAM-B3LYP	3243.16345576	3243.16872671
B3LYP	3245.606080	3245.60611414

**Table S13** Computed energy values for all three possible spin states of  $[1^{ox1}]^{1+}$ , using CAM-B3LYP functional

$-E_{HS}$ (a.u.) $S = 3/2$	$-E_{LS1}$ (a.u.) $Ms = 1/2$	$-E_{LS2}$ (a.u.) $Ms = 1/2$
3243.95672395	3243.95542340	3243.98051692

**Table S14** TD-DFT-calculated electronic transitions of **1**, using CAM-B3LYP

Excitation energy (eV)	$\lambda$ (nm)	$f$	Transition	Assignment
1.0943	1133	0.1678	$\alpha$ -H[~85%L] → $\alpha$ -L[~77%L] (45%)	Inter-ligand CT in $(L^{ISQ})^{\bullet-}$ ring
			$\alpha$ -H-1[~72%L] → $\alpha$ -L[~77%L] (11%)	Intra-ligand CT in $(L^{ISQ})^{\bullet-}$ ring
			$\beta$ -H[~84%L] → $\beta$ -L[~81%L] (14%)	Inter-ligand CT in $(L^{ISQ})^{\bullet-}$ ring
1.4030	884	0.0496	$\alpha$ -H-1[~72%L] → $\alpha$ -L[~77%L] (46%)	Intra-ligand CT in $(L^{ISQ})^{\bullet-}$ ring
			$\beta$ -H[~84%L] → $\beta$ -L[~81%L] (28%)	Inter-ligand CT in $(L^{ISQ})^{\bullet-}$ ring
1.5419	804	0.0649	$\alpha$ -H-1[~72%L] → $\alpha$ -L[~77%L] (15%)	Intra-ligand CT in $(L^{ISQ})^{\bullet-}$ ring
			$\beta$ -H-1[~70%L] → $\beta$ -L[~81%L] (61%)	Intra-ligand CT in $(L^{ISQ})^{\bullet-}$ ring and minor MLCT involving Ru → $(L^{ISQ})^{\bullet-}$
1.9519	635	0.0206	$\beta$ -H-3[~54%M] → $\beta$ -L [~81%L] (38%)	MLCT involving Ru → $(L^{ISQ})^{\bullet-}$ , along with intra-ligand CT in $(L^{ISQ})^{\bullet-}$ ring
			$\beta$ -H-2[~68%M] → $\beta$ -L [~81%L] (38%)	MLCT involving Ru → $(L^{ISQ})^{\bullet-}$ , along with inter-ligand CT in $(L^{ISQ})^{\bullet-}$ ring
2.3352	531	0.0383	$\alpha$ -H-5[~61%L] → $\alpha$ -L[~77%L] (18%)	Inter-ligand CT in $(L^{ISQ})^{\bullet-}$ ring and MLCT involving Ru → $(L^{ISQ})^{\bullet-}$
			$\alpha$ -H-4[~53%L] → $\alpha$ -L [~77%L] (12%)	Inter-ligand CT in $(L^{ISQ})^{\bullet-}$ ring and MLCT involving Ru → $(L^{ISQ})^{\bullet-}$

			$\alpha$ -H-3[~53%L] → $\alpha$ -L[~77%L] (24%)	Intra-ligand CT in $(L^{ISQ})^{\bullet-}$ ring, along with MLCT involving Ru → $(L^{ISQ})^{\bullet-}$
			$\alpha$ -H-2[~62%L] → $\alpha$ -L[~77%L] (20%)	Inter-ligand CT in $(L^{ISQ})^{\bullet-}$ ring and MLCT involving Ru → $(L^{ISQ})^{\bullet-}$
2.3965	517	0.0316	$\beta$ -H-5[~57%L] → $\beta$ -L[~81%L] (22%)	Inter-ligand CT in $(L^{ISQ})^{\bullet-}$ ring and MLCT involving Ru → $(L^{ISQ})^{\bullet-}$
			$\beta$ -H-3[~54%L] → $\beta$ -L[~81%L] (31%)	Intraligand CT in $(L^{ISQ})^{\bullet-}$ ring, along with MLCT involving Ru → $(L^{ISQ})^{\bullet-}$
			$\beta$ -H-2[~68%L] → $\beta$ -L[~81%L] (23%)	Inter-ligand CT in $(L^{ISQ})^{\bullet-}$ ring and MLCT involving Ru → $(L^{ISQ})^{\bullet-}$
2.8435	436	0.0686	$\alpha$ -H-4[~53%L] → $\alpha$ -L[~77%L] (10%)	Inter-ligand CT in $(L^{ISQ})^{\bullet-}$ ring and MLCT involving Ru → $(L^{ISQ})^{\bullet-}$
			$\alpha$ -H-3[~53%L] → $\alpha$ -L [~77%L] (12%)	Intra-ligand CT in $(L^{ISQ})^{\bullet-}$ ring, along with MLCT involving Ru → $(L^{ISQ})^{\bullet-}$
			$\beta$ -H-4[~52%L] → $\beta$ -L[~81%L] (25%)	MLCT involving Ru → $(L^{ISQ})^{\bullet-}$
			$\beta$ -H-3[~54%L] → $\beta$ -L[~81%L] (12%)	Intra-ligand CT in $(L^{ISQ})^{\bullet-}$ ring, along with MLCT involving Ru → $(L^{ISQ})^{\bullet-}$
3.3633	357	0.1171	$\alpha$ -H[~85%L] → $\alpha$ -L+1[~58%L] (13%)	$(L^{ISQ})^{\bullet-}$ → amino-thioether
			$\alpha$ -H[~85%L] → $\alpha$ -L+3[~47%L](8%)	CT in $(L^{ISQ})^{\bullet-}$ ring
			$\beta$ -H[~84%L] → $\beta$ -L+1[~57%L] (10%)	CT $(L^{ISQ})^{\bullet-}$ → amino-thioether
3.3633	339	0.0782	$\alpha$ -H-5[~61%L] → $\alpha$ -L[~77%L] (11%)	Inter-ligand CT in $(L^{ISQ})^{\bullet-}$ ring and MLCT involving Ru →

---

	(L <sup>ISQ</sup> ) <sup>•-</sup>
$\alpha$ -H[~85%L] → $\alpha$ -L+3[~47%L] (16%)	CT in (L <sup>ISQ</sup> ) <sup>•-</sup> ring
$\alpha$ -H[~85%L] → $\alpha$ -L+1[~58%L] (7%)	CT involving (L <sup>ISQ</sup> ) <sup>•-</sup> → amino-thioether

---

**Table S15** TD-DFT-calculated electronic transitions of **1**, using B3LYP

Excitation energy (eV)	$\lambda$ (nm)	$f$	Transition	Assignment
1.1356	1091	0.1811	$\alpha$ -H[~95%L] → $\alpha$ -L[~70%L] (44%)	Inter-ligand charge-transfer (CT) between two ligands involving $(L^{AP})^{2-}/(L^{ISQ})^{\bullet-}$ with minor intra-ligand CT in $(L^{ISQ})^{\bullet-}$ and ligand-to-metal (LM)CT from $(L^{ISQ})^{\bullet-} \rightarrow Ru$
			$\beta$ -H[~95%L] → $\beta$ -L[~70%L] (43%)	Inter-ligand CT between two ligands involving $(L^{AP})^{2-}/(L^{ISQ})^{\bullet-}$ with minor intra-ligand CT in $(L^{ISQ})^{\bullet-}$ and LMCT from $(L^{ISQ})^{\bullet-} \rightarrow Ru$
1.6941	731	0.0641	$\alpha$ -H-2[~66%L] → $\alpha$ -L[~70%L] (33%)	Combination of inter- and intra-ligand CT involving $(L^{AP})^{2-}/(L^{ISQ})^{\bullet-}$ along with some amount of metal-to-ligand (ML)CT, involving $Ru \rightarrow (L^{ISQ})^{\bullet-}$
			$\beta$ -H-2[~64%L] → $\beta$ -L[~70%L] (30%)	Combination of inter- and intra-ligand CT involving $(L^{AP})^{2-}/(L^{ISQ})^{\bullet-}$ along with some amount of MLCT, involving $Ru \rightarrow (L^{ISQ})^{\bullet-}$
			$\alpha$ -H-4[~53%L] → $\alpha$ -L[~70%L] (7%)	Inter-ligand CT between two ligands involving $(L^{AP})^{2-}/(L^{ISQ})^{\bullet-}$ along with significant amount of MLCT, involving $Ru \rightarrow (L^{ISQ})^{\bullet-}$
2.1116	587	0.0479	$\alpha$ -H-5[~54%L] → $\alpha$ -L[~70%L] (24%)	Combination of intra and inter-ligand CT involving $(L^{AP})^{2-}/(L^{ISQ})^{\bullet-}$ and significant MLCT, involving $Ru \rightarrow (L^{ISQ})^{\bullet-}$
			$\alpha$ -H-3[~58%L] →	Combination of intra- and inter-

			$\alpha$ -L[~70%L] (18%)	ligand CT involving $(L^{AP})^{2-}/(L^{ISQ})^{\cdot-}$ and MLCT, involving $Ru \rightarrow (L^{ISQ})^{\cdot-}$
			$\beta$ -H-5[~51%L] $\rightarrow$ $\beta$ -L[~70%L] (26%)	Combination of intra- and inter-ligand CT involving $(L^{AP})^{2-}/(L^{ISQ})^{\cdot-}$ and significant MLCT, involving $Ru \rightarrow (L^{ISQ})^{\cdot-}$
			$\beta$ -H-3[~59%L] $\rightarrow$ $\beta$ -L[~70%L] (12%)	Inter- and intra-ligand CT involving $(L^{AP})^{2-}/(L^{ISQ})^{\cdot-}$ with substantial amount of MLCT, involving $Ru \rightarrow (L^{ISQ})^{\cdot-}$
2.2944	540	0.0405	$\beta$ -H-3[~59%M] $\rightarrow$ $\beta$ -L[~70%L] (10%)	Inter- and intra-ligand CT involving $(L^{AP})^{2-}/(L^{ISQ})^{\cdot-}$ with substantial amount of MLCT, involving $Ru \rightarrow (L^{ISQ})^{\cdot-}$
			$\alpha$ -H-5[~54%L] $\rightarrow$ $\alpha$ -L[~70%L] (24%)	Combination of intra- and inter-ligand CT involving $(L^{AP})^{2-}/(L^{ISQ})^{\cdot-}$ and significant MLCT, involving $Ru \rightarrow (L^{ISQ})^{\cdot-}$
			$\alpha$ -H-3[~58%L] $\rightarrow$ $\alpha$ -L[~70%L] (14%)	Combination of intra- and inter-ligand CT involving $(L^{AP})^{2-}/(L^{ISQ})^{\cdot-}$ and MLCT, involving $Ru \rightarrow (L^{ISQ})^{\cdot-}$
2.3975	517	0.0775	$\alpha$ -H-5[~54%L] $\rightarrow$ $\alpha$ -L[~70%L] (10%)	Combination of intra- and inter-ligand CT involving $(L^{AP})^{2-}/(L^{ISQ})^{\cdot-}$ and significant MLCT, involving $Ru \rightarrow (L^{ISQ})^{\cdot-}$
			$\alpha$ -H-4[~53%L] $\rightarrow$ $\alpha$ -L[~70%L] (26%)	Inter-ligand CT between two ligands involving $(L^{AP})^{2-}/(L^{ISQ})^{\cdot-}$ along with significant amount of MLCT, involving $Ru \rightarrow (L^{ISQ})^{\cdot-}$
			$\beta$ -H-5[~51%L] $\rightarrow$	Combination of intra- and inter-

			$\beta$ -L[~70%L] (20%)	ligand CT involving $(L^{AP})^{2-}/(L^{ISQ})^{\bullet-}$ and significant MLCT, involving $Ru \rightarrow (L^{ISQ})^{\bullet-}$
			$\beta$ -H-4[~53%L] $\rightarrow$ $\beta$ -L[~70%L] (16%)	Inter-ligand CT involving $(L^{AP})^{2-}/(L^{ISQ})^{\bullet-}$ with substantial amount of MLCT, involving $Ru \rightarrow (L^{ISQ})^{\bullet-}$
2.7755	446	0.0118	$\beta$ -H-6[~95%L] $\rightarrow$ $\beta$ -L[~70%L] (11%)	Inter- and intra-ligand CT from amino-thioether and $(L^{AP})^{2-}/(L^{ISQ})^{\bullet-}$ ring $\rightarrow (L^{ISQ})^{\bullet-}$ , along with LMCT, involving $(L^{AP})^{2-}/(L^{ISQ})^{\bullet-} \rightarrow Ru$
			$\beta$ -H[~95%L] $\rightarrow$ $\beta$ -L+1[~70%L] (29%)	Intra-ligand CT from $(L^{AP})^{2-}/(L^{ISQ})^{\bullet-} \rightarrow$ amino-thioether part, along with LMCT, involving $(L^{AP})^{2-}/(L^{ISQ})^{\bullet-} \rightarrow Ru$
			$\alpha$ -H-6[~96%L] $\rightarrow$ $\alpha$ -L[~70%L] (14%)	Inter- and intra-ligand CT from amino-thioether and $(L^{AP})^{2-}/(L^{ISQ})^{\bullet-} \rightarrow (L^{ISQ})^{\bullet-}$ , along with LMCT, involving $(L^{AP})^{2-}/(L^{ISQ})^{\bullet-} \rightarrow Ru$
			$\alpha$ -H[~95%L] $\rightarrow$ $\alpha$ -L+1[~71%L] (32%)	Intra-ligand CT from $(L^{AP})^{2-}/(L^{ISQ})^{\bullet-} \rightarrow$ amino-thioether part, along with LMCT, involving $(L^{AP})^{2-}/(L^{ISQ})^{\bullet-} \rightarrow Ru$
2.8715	431	0.0393	$\alpha$ -H[~95%L] $\rightarrow$ $\alpha$ -L+1[~71%L] (31%)	Intra-ligand CT from $(L^{AP})^{2-}/(L^{ISQ})^{\bullet-} \rightarrow$ amino-thioether part, along with LMCT, involving $(L^{AP})^{2-}/(L^{ISQ})^{\bullet-} \rightarrow Ru$
			$\beta$ -H[~95%L] $\rightarrow$ $\beta$ -L+1[~70%L]	Intra-ligand CT from $(L^{AP})^{2-}/(L^{ISQ})^{\bullet-} \rightarrow$ amino-thioether part, along with LMCT,

			(31%)	involving $(L^{AP})^{2-}/(L^{ISQ})^{\bullet-} \rightarrow Ru$
3.0430	407	0.0142	$\alpha$ -H-7[~91%L] → $\alpha$ -L[~70%L] (12%)	Phenyl-amino-thioether → $(L^{ISQ})^{\bullet-}$ along with LMCT, involving $(L^{AP})^{2-}/(L^{ISQ})^{\bullet-} \rightarrow Ru$
			$\alpha$ -H-6[~98%L] → $\alpha$ -L[~70%L] (31%)	Inter- and intra-ligand CT from amino-thioether and $(L^{AP})^{2-}/(L^{ISQ})^{\bullet-} \rightarrow (L^{ISQ})^{\bullet-}$ , along with LMCT, involving $(L^{AP})^{2-}/(L^{ISQ})^{\bullet-} \rightarrow Ru$
			$\beta$ -H-6[~98%L] → $\beta$ -L[~70%L] (30%)	Inter- and intra-ligand CT from amino-thioether and $(L^{AP})^{2-}$ ring → $(L^{AP})^{2-}/(L^{ISQ})^{\bullet-}$ , along with LMCT, involving $(L^{AP})^{2-}/(L^{ISQ})^{\bullet-} \rightarrow Ru$
3.0525	406	0.0209	$\alpha$ -H[~95%L] → $\alpha$ -L+2[~74%L] (13%)	CT from $(L^{AP})^{2-}/(L^{ISQ})^{\bullet-} \rightarrow$ amino-thioether with subsequent LMCT, involving $(L^{AP})^{2-}/(L^{ISQ})^{\bullet-} \rightarrow Ru$
			$\alpha$ -H[~95%L] → $\alpha$ -L+3[~82%L] (23%)	CT from $(L^{AP})^{2-}/(L^{ISQ})^{\bullet-} \rightarrow$ amino-thioether with subsequent LMCT, involving $(L^{AP})^{2-}/(L^{ISQ})^{\bullet-} \rightarrow Ru$
			$\beta$ -H[~95%L] → $\beta$ -L+2[~75%L] (16%)	CT from $(L^{AP})^{2-}/(L^{ISQ})^{\bullet-} \rightarrow$ amino-thioether, along with LMCT, involving $(L^{AP})^{2-}/(L^{ISQ})^{\bullet-} \rightarrow Ru$
			$\beta$ -H[~95%L] → $\beta$ -L+3[~80%L] (25%)	CT from $(L^{AP})^{2-}/(L^{ISQ})^{\bullet-} \rightarrow$ amino-thioether, along with LMCT, involving $(L^{AP})^{2-}/(L^{ISQ})^{\bullet-} \rightarrow Ru$
			$\alpha$ -H-7[~91%L] →	Phenyl-amino-thioether →

3.1694	391	0.0208	$\alpha$ -L[~70%L] (26%)	(L <sup>ISQ</sup> ) <sup>•-</sup> , along with LMCT, involving (L <sup>AP</sup> ) <sup>2-</sup> /(L <sup>ISQ</sup> ) <sup>•-</sup> → Ru
			$\beta$ -H-7[~91%L] → $\beta$ -L[~70%L] (23%)	Phenyl-amino-thioether → (L <sup>ISQ</sup> ) <sup>•-</sup> with subsequent LMCT, involving (L <sup>AP</sup> ) <sup>2-</sup> /(L <sup>ISQ</sup> ) <sup>•-</sup> → Ru
3.2052	386	0.0594	$\alpha$ -H-8[~94%L] → $\alpha$ -L[~70%L] (16%)	Inter-ligand CT involving (L <sup>AP</sup> ) <sup>2-</sup> /(L <sup>ISQ</sup> ) <sup>•-</sup> with subsequent LMCT, involving (L <sup>AP</sup> ) <sup>2-</sup> /(L <sup>ISQ</sup> ) <sup>•-</sup> → Ru
			$\alpha$ -H-7[~91%L] → $\alpha$ -L[~70%L] (18%)	Phenyl-amino-thioether → (L <sup>ISQ</sup> ) <sup>•-</sup> with subsequent LMCT, involving (L <sup>AP</sup> ) <sup>2-</sup> /(L <sup>ISQ</sup> ) <sup>•-</sup> → Ru
			$\beta$ -H-8[~95%L] → $\beta$ -L[~70%L] (17%)	Inter-ligand CT involving (L <sup>AP</sup> ) <sup>2-</sup> /(L <sup>ISQ</sup> ) <sup>•-</sup> with subsequent LMCT, involving (L <sup>AP</sup> ) <sup>2-</sup> /(L <sup>ISQ</sup> ) <sup>•-</sup> → Ru
			$\beta$ -H-7[~91%L] → $\beta$ -L[~70%L] (17%)	Phenyl-amino-thioether → (L <sup>ISQ</sup> ) <sup>•-</sup> with subsequent LMCT, involving (L <sup>AP</sup> ) <sup>2-</sup> /(L <sup>ISQ</sup> ) <sup>•-</sup> → Ru

**Table S16** TD-DFT-calculated electronic transitions of  $[1^{Ox1}]^{1+}$ , using CAM-B3LYP

Excitation energy (eV)	$\lambda$ (nm)	$f$	Transition	Assignment
0.8657	1432	0.0497	$\alpha$ -H-4[~60%L] → $\alpha$ -L[~56%L] (19%) $\alpha$ -H-2[~82%L] → $\alpha$ -L[~56%L] (10%) $\alpha$ -H[~96%L] → $\alpha$ -L[~56%L] (54%)	Inter-ligand CT in $(L^{IBQ})^0$ ring to $(L^{ISQ})^{\bullet-}$ CT in $(L^{ISQ})^{\bullet-}$ with LMCT involving $(L^{ISQ})^{\bullet-} \rightarrow Ru$
1.3714	904	0.039	$\beta$ -H[~80%L] → $\beta$ -L[~94%L] (43%) $\alpha$ -H[~96%L] → $\alpha$ -L[~56%L] (24%) $\alpha$ -H-2[~82%L] → $\alpha$ -L[~56%L] (10%)	Combination of CT in $(L^{ISQ})^{\bullet-}$ and LMCT involving $(L^{ISQ})^{\bullet-} \rightarrow Ru$
1.4816	837	0.0592	$\alpha$ -H-4[~60%L] → $\alpha$ -L[~56%L] (30%) $\alpha$ -H[~96%L] → $\alpha$ -L[~56%L] (16%) $\beta$ -H[~80%L] → $\beta$ -L[~94%L] (23%)	Intra-ligand CT $(L^{ISQ})^{\bullet-}$ ring
1.8505	670	0.0125	$\alpha$ -H-3[~65%L] → $\alpha$ -L[~54%L] (51%) $\alpha$ -H-1[~70%L] → $\alpha$ -L [~54%L] (19%)	Combination of CT in $(L^{ISQ})^{\bullet-}$ and LMCT involving $(L^{ISQ})^{\bullet-} \rightarrow Ru$

2.4579	504	0.0323	$\beta$ -H-5[~79%L] → $\beta$ -L[~94%L] (28%) $\beta$ -H-1[~91%L] → $\beta$ -L+1[~87%L] (17%) $\beta$ -H[~80%L] → $\beta$ -L[~94%L] (12%)	Intra-ligand CT in $(L^{ISQ})^{\cdot-}$ ring with small amount of MLCT involving Ru → $(L^{ISQ})^{\cdot-}$ ring Intra-ligand CT within $(L^{ISQ})^{\cdot-}$ Intra-ligand CT $(L^{ISQ})^{\cdot-}$ ring
2.6661	465	0.07	$\beta$ -H-9[~93%L] → $\beta$ -L+1[~87%L] (11%) $\beta$ -H-8[~67%L] → $\beta$ -L[~94%L] (16%) $\beta$ -H-2[~57%L] → $\beta$ -L+1[~87%L] (10%)	Intra-ligand CT in phenyl ring of $(L^{ISQ})^{\cdot-}$ ring Inter-ligand CT involving phenyl ring of $(L^{ISQ})^{\cdot-}$ ring and MLCT involving Ru → $(L^{ISQ})^{\cdot-}$ ring CT involving phenyl ring appended with thioether → $(L^{ISQ})^{\cdot-}$ ring, along with MLCT involving Ru → $(L^{ISQ})^{\cdot-}$ ring
2.6911	460	0.0901	$\beta$ -H-9[~93%L] → $\beta$ -L[~94%L] (22%) $\beta$ -H-5[~80%L] → $\beta$ -L+1[~87%L] (12%) $\beta$ -H-2[~57%L] → $\beta$ -L[~94%L] (10%) $\beta$ -H[~80%L] → $\beta$ -L+1[~87%L] (12%)	Intra-ligand CT in phenyl ring of $(L^{ISQ})^{\cdot-}$ ring Intra-ligand CT involving $(L^{ISQ})^{\cdot-}$ ring CT involving phenyl ring appended with thioether → $(L^{ISQ})^{\cdot-}$ ring with MLCT involving Ru → $(L^{ISQ})^{\cdot-}$ ring Intra-ligand CT within $(L^{ISQ})^{\cdot-}$ ring
2.8939	428	0.0188	$\beta$ -H-12[~65%L] → $\beta$ -L[~94%L] (14%) $\beta$ -H-10[~74%L] → $\beta$ -L[~94%L] (18%) $\beta$ -H-3[~71%L] → $\beta$ -L[~94%L] (24%)	MLCT involving Ru → $(L^{ISQ})^{\cdot-}$ and CT involving amino-thioether → $(L^{ISQ})^{\cdot-}$ ring CT involving amino-thioether → $(L^{ISQ})^{\cdot-}$ ring and MLCT involving Ru → $(L^{ISQ})^{\cdot-}$ CT involving phenyl ring appended with thioether → $(L^{ISQ})^{\cdot-}$ ring and MLCT involving Ru → $(L^{ISQ})^{\cdot-}$
3.0546	406	0.1026	$\alpha$ -H-9[~60%L] → $\alpha$ -L[~54%L] (12%) $\alpha$ -H-1[~70%L] → $\alpha$ -L[~54%L] (11%)	LMCT involving amino-thioether functionality of $(L^{ISQ})^{\cdot-}$ → Ru, along with CT from amino- thioether → $(L^{ISQ})^{\cdot-}$ ring
CT in $(L^{ISQ})^{\cdot-}$ and LMCT				

				involving $(L^{ISQ})^{\bullet-}$ ring $\rightarrow$ Ru
3.0847	401	0.1287	$\alpha$ -H-2[~82%L] $\rightarrow$ $\alpha$ -L[~54%L] (12%)	CT in $(L^{ISQ})^{\bullet-}$ with LMCT involving $(L^{ISQ})^{\bullet-} \rightarrow$ Ru
			$\beta$ -H-2[~57%L] $\rightarrow$ $\beta$ -L+1[~87%L] (10%)	CT involving phenyl ring appended with thioether $\rightarrow$ $(L^{ISQ})^{\bullet-}$ ring with MLCT involving Ru $\rightarrow$ $(L^{ISQ})^{\bullet-}$ ring
			$\beta$ -H-3[~71%L] $\rightarrow$ $\beta$ -L[~94%L] (24%)	CT involving phenyl ring appended with thioether $\rightarrow$ $(L^{ISQ})^{\bullet-}$ ring and MLCT involving Ru $\rightarrow$ $(L^{ISQ})^{\bullet-}$
3.6367	340	0.016	$\alpha$ -H[~96%L] $\rightarrow$ $\alpha$ -L+1[~77%L] (11%)	CT in $(L^{ISQ})^{\bullet-}$ ring and LMCT involving $(L^{ISQ})^{\bullet-}$ ring $\rightarrow$ Ru
			$\alpha$ -H[~96%L] $\rightarrow$ $\alpha$ -L+2[~70%L] (18%)	CT in $(L^{ISQ})^{\bullet-}$ ring and LMCT involving $(L^{ISQ})^{\bullet-} \rightarrow$ Ru
			$\beta$ -H-3[~71%L] $\rightarrow$ $\beta$ -L[~94%L] (24%)	CT involving phenyl ring appended with thioether $\rightarrow$ $(L^{ISQ})^{\bullet-}$ ring and MLCT involving Ru $\rightarrow$ $(L^{ISQ})^{\bullet-}$

**Table 17** TD-DFT-calculated electronic transitions of  $[1^{OX1}]^{1+}$ , using B3LYP

Excitation energy (eV)	$\lambda$ (nm)	$f$	Transition	Assignment
0.8100	1530	0.065	$\alpha\text{-H}[\sim 95\%\text{L}] \rightarrow \alpha\text{-L}[\sim 62\%\text{L}]$ (89%)	Intra-ligand (CT) in $(\text{L}^{\text{ISQ}})^{\cdot-}$ ring and LMCT involving $(\text{L}^{\text{ISQ}})^{\cdot-} \rightarrow \text{Ru}$
1.3413	924	0.021	$\beta\text{-H}[\sim 68\%\text{L}] \rightarrow \beta\text{-L}[\sim 96\%\text{L}]$ (10%)	Intra-ligand CT in $(\text{L}^{\text{ISQ}})^{\cdot-}$ along with MLCT involving $\text{Ru} \rightarrow (\text{L}^{\text{ISQ}})^{\cdot-}$
			$\alpha\text{-H-3}[\sim 62\%\text{L}] \rightarrow \alpha\text{-L}[\sim 62\%\text{L}]$ (10%)	Intra-ligand CT in $(\text{L}^{\text{ISQ}})^{\cdot-}$
			$\alpha\text{-H-2}[\sim 57\%\text{L}] \rightarrow \alpha\text{-L}[\sim 62\%\text{L}]$ (50%)	Intra-ligand CT in $(\text{L}^{\text{ISQ}})^{\cdot-}$ and MLCT involving $\text{Ru} \rightarrow (\text{L}^{\text{ISQ}})^{\cdot-}$
1.4045	882	0.043	$\alpha\text{-H-1}[\sim 62\%\text{L}] \rightarrow \alpha\text{-L}[\sim 62\%\text{L}]$ (12%)	Intra-ligand CT in $(\text{L}^{\text{ISQ}})^{\cdot-}$
			$\beta\text{-H-1}[\sim 76\%\text{L}] \rightarrow \beta\text{-L}[\sim 96\%\text{L}]$ (64%)	Combination of CT in $(\text{L}^{\text{ISQ}})^{\cdot-}$ with appreciable amount of MLCT involving $\text{Ru} \rightarrow (\text{L}^{\text{ISQ}})^{\cdot-}$
2.0140	615	0.1287	$\alpha\text{-H-2}[\sim 57\%\text{L}] \rightarrow \alpha\text{-L}[\sim 62\%\text{L}]$ (13%)	Intra-ligand CT in $(\text{L}^{\text{ISQ}})^{\cdot-}$ involving Ru center with appreciable amount of MLCT involving $\text{Ru} \rightarrow (\text{L}^{\text{ISQ}})^{\cdot-}$
			$\beta\text{-H-3}[\sim 51\%\text{M}] \rightarrow \beta\text{-L}[\sim 96\%\text{L}]$ (39%)	MLCT involving $\text{Ru} \rightarrow (\text{L}^{\text{ISQ}})^{\cdot-}$
			$\beta\text{-H-2}[\sim 48\%\text{M}] \rightarrow \beta\text{-L+1}[\sim 80\%\text{L}]$ (20%)	MLCT involving $\text{Ru} \rightarrow (\text{L}^{\text{ISQ}})^{\cdot-}$
			$\beta\text{-H-1}[\sim 76\%\text{L}] \rightarrow \beta\text{-L}[\sim 96\%\text{L}]$ (17%)	Combination of CT in $(\text{L}^{\text{ISQ}})^{\cdot-}$ , along with appreciable amount of MLCT involving $\text{Ru} \rightarrow (\text{L}^{\text{ISQ}})^{\cdot-}$

2.2078	561	0.041	$\alpha$ -H-4[~62%L] → $\alpha$ -L[~62%L] (12%)	Intra-ligand CT in $(L^{ISQ})^{\cdot-}$ , along with small amount of MLCT involving Ru → $(L^{ISQ})^{\cdot-}$
			$\alpha$ -H-3[~62%L] → $\alpha$ -L[~62%L] (13%)	Intra-ligand CT in $(L^{ISQ})^{\cdot-}$
			$\beta$ -H-4[~70%L] → $\beta$ -L+1[~80%L] (55%)	Intra-ligand CT in $(L^{ISQ})^{\cdot-}$ , along with small amount of MLCT involving Ru → $(L^{ISQ})^{\cdot-}$
2.3353	530	0.047	$\beta$ -H-2[~48%M] → $\beta$ -L+1[~80%L] (35%)	MLCT involving Ru → $(L^{ISQ})^{\cdot-}$
			$\beta$ -H-1[~76%L] → $\beta$ -L+1 [~80%L] (22%)	Intra-ligand CT in $(L^{ISQ})^{\cdot-}$ , along with small amount of MLCT involving Ru → $(L^{ISQ})^{\cdot-}$
2.3509	527	0.055	$\beta$ -H-9[~96%L] → $\beta$ -L[~96%L] (30%)	Intra-ligand CT in $(L^{ISQ})^{\cdot-}$
			$\beta$ -H-5[~80%L] → $\beta$ -L[~96%L] (36%)	Intra-ligand CT from phenyl-imino-thioether to $(L^{ISQ})^{\cdot-}$
2.4461	506	0.026	$\alpha$ -H-10[~65%L] → $\alpha$ -L[~94%L] (10%)	Intra-ligand CT in $(L^{ISQ})^{\cdot-}$ and MLCT involving Ru → $(L^{ISQ})^{\cdot-}$
			$\beta$ -H-10[~84%L] → $\beta$ -L[~96%L] (18%)	Intra-ligand CT involving phenyl-imino-thioether moiety → $(L^{ISQ})^{\cdot-}$ with minor contribution of MLCT involving Ru → $(L^{ISQ})^{\cdot-}$
			$\beta$ -H-8[~73%L] → $\beta$ -L[~96%L] (26%)	CT from phenyl ring appended to thioether → $(L^{ISQ})^{\cdot-}$ and minor MLCT involving Ru → $(L^{ISQ})^{\cdot-}$
				CT from phenyl ring appended to thioether → $(L^{ISQ})^{\cdot-}$ and minor

			$\beta$ -H-7[~80%L] → $\beta$ -L[~96%L] (14%)	MLCT involving Ru → (L <sup>ISQ</sup> ) <sup>•-</sup>
2.5426	487	0.032	$\beta$ -H-9[~96%L] → $\beta$ -L[~96%L] (12%)	Intraligand CT in (L <sup>ISQ</sup> ) <sup>•-</sup>
			$\beta$ -H-4[~70%L] → $\beta$ -L+1[~54%L] (14%)	Intraligand CT in (L <sup>ISQ</sup> ) <sup>•-</sup> , along with small amount of MLCT involving Ru → (L <sup>ISQ</sup> ) <sup>•-</sup>
			$\beta$ -H-3[~51%M] → $\beta$ -L+1[~80%L] (24%)	MLCT involving Ru → (L <sup>ISQ</sup> ) <sup>•-</sup>
2.5507	486	0.051	$\beta$ -H-1[~76%L] → $\beta$ -L[~96%L] (20%)	Combination of CT in (L <sup>ISQ</sup> ) <sup>•-</sup> with appreciable amount of MLCT involving Ru → (L <sup>ISQ</sup> ) <sup>•-</sup>
			$\beta$ -H-9[~96%L] → $\beta$ -L[~96%L] (18%)	Intra-ligand CT in (L <sup>ISQ</sup> ) <sup>•-</sup>
			$\beta$ -H-5[~80%L] → $\beta$ -L[~96%L] (26%)	Intra-ligand CT from phenyl-imino-thioether to (L <sup>ISQ</sup> ) <sup>•-</sup>
2.8318	437	0.03	$\beta$ -H-3[~51%M] → $\beta$ -L+1[~80%L] (20%)	MLCT involving Ru → (L <sup>ISQ</sup> ) <sup>•-</sup>
			$\alpha$ -H-9[~60%L] → $\alpha$ -L[~63%L] (37%)	CT from phenyl ring appended to thioether → (L <sup>ISQ</sup> ) <sup>•-</sup> and appreciable MLCT involving Ru → (L <sup>ISQ</sup> ) <sup>•-</sup>
			$\alpha$ -H-7[~97%L] → $\alpha$ -L[~63%L] (10%)	CT from phenyl ring appended to thioether → (L <sup>ISQ</sup> ) <sup>•-</sup> and LMCT involving phenyl ring appended to thioether → Ru
			$\alpha$ -H-5[~78%L] → $\alpha$ -L[~63%L] (11%)	Intra-ligand CT involving (L <sup>ISQ</sup> ) <sup>•-</sup> -imino-thioether appended phenyl

ring →  $(L^{ISQ})^{\bullet-}$  and LMCT involving  
 $(L^{ISQ})^{\bullet-}$ -imino-thioether appended  
phenyl ring → Ru

**Table S18** TD-DFT-calculated electronic transitions of  $[1^{OX2}]^{2+}$ , using CAM-B3LYP

Excitation energy	$\lambda$ (nm)	$F$	Transition	Assignment
1.1920	1040	0.0237	$\alpha/\beta\text{-H}[\sim 74\%L] \rightarrow \alpha/\beta\text{-L}[\sim 96\%L]$ (44%)	Intra-ligand CT within $(L^{IBQ})^0$ ring along with minor contribution of MLCT involving Ru to $(L^{IBQ})^0$ ring
1.5365	806	0.0459	$\alpha/\beta\text{-H-7}[\sim 66\%L] \rightarrow \alpha/\beta\text{-L}[\sim 96\%L]$ (18%)	Intra-ligand CT from aminothioether moiety to $(L^{IBQ})^0$ ring, with significant contribution of MLCT involving Ru to $(L^{IBQ})^0$
			$\alpha/\beta\text{-H-1}[\sim 89\%L] \rightarrow \alpha/\beta\text{-L}[\sim 96\%L]$ (25%)	Intra-ligand CT within $(L^{IBQ})^0$ ring
1.6797	738	0.0483	$\alpha/\beta\text{-H}[\sim 74\%L] \rightarrow \alpha/\beta\text{-L+1}[\sim 75\%L]$ (29%)	Intra-ligand CT within $(L^{IBQ})^0$ ring
1.8546	668	0.01520	$\alpha/\beta\text{-H-6}[\sim 64\%L] \rightarrow \alpha/\beta\text{-L}[\sim 96\%L]$ (20%) $\alpha/\beta\text{-H-2}[\sim 66\%L]$	Intra-liand CT within $(L^{IBQ})^0$ with significant contribution of MLCT involving Ru to $(L^{IBQ})^0$ ring CT from appended phenyl ring to $(L^{IBQ})^0$ ring, along with

			$\rightarrow$ $\alpha/\beta-L[\sim 96\%L]$ (11%)	MLCT involving Ru to $(L^{IBQ})^0$ ring
2.0458	606	0.1133	$\alpha/\beta-H-7[\sim 66\%L]$ $\rightarrow$ $\alpha/\beta-L+1[\sim 75\%L]$ (15%) $\alpha/\beta-H-1[\sim 89\%L] \rightarrow$ $\alpha/\beta-L+1[\sim 75\%L]$ (10%)	Intra-ligand CT to $(L^{IBQ})^0$ ring from phenyl aminothioether moiety with MLCT involving Ru $\rightarrow (L^{IBQ})^0$ ring Intra-ligand CT within $(L^{IBQ})^0$ ring with small contribution of LMCT involving $(L^{IBQ})^0$ ring $\rightarrow$ Ru
2.2110	560	0.1080	$\alpha/\beta-H-8[\sim 53\%L] \rightarrow$ $\alpha/\beta-L[\sim 96\%L]$ (11%) $\alpha/\beta-H-6[\sim 64\%L] \rightarrow$ $\alpha/\beta-L[\sim 96\%L]$ (13%)	CT within $(L^{IBQ})^0$ with significant contribution of MLCT involving Ru to $(L^{IBQ})^0$ ring Intra-liand CT within $(L^{IBQ})^0$ with significant contribution of MLCT involving Ru to $(L^{IBQ})^0$
2.5851	479	0.1053	$\alpha/\beta-H-9[\sim 95\%L] \rightarrow$ $\alpha/\beta-L[\sim 96\%L]$ (20%)	Intra-ligand CT in phenyl- $(L^{IBQ})^0$ ring from phenylaminothioether moiety
2.7462	451	0.1773	$\alpha/\beta-H-10[\sim 87\%L]$ $\rightarrow$ $\alpha/\beta-L[\sim 96\%L]$ (7%) $\alpha/\beta-H-8[\sim 53\%L] \rightarrow$ $\alpha/\beta-L[\sim 96\%L]$ (9%)  $\alpha/\beta-H-2[\sim 66\%L]$ $\rightarrow$ $\alpha/\beta-L[\sim 96\%L]$ (6%)	Intra-ligand CT within $(L^{IBQ})^0$  CT within $(L^{IBQ})^0$ with significant contribution of MLCT involving Ru to $(L^{IBQ})^0$ ring  CT from appended phenyl ring to $(L^{IBQ})^0$ ring along with MLCT involving Ru to $(L^{IBQ})^0$
2.8125	440	0.1686	$\alpha/\beta-H-9[\sim 95\%L] \rightarrow$ $\alpha/\beta-L[\sim 96\%L]$ (20%)	Intra-ligand CT in phenyl- $(L^{IBQ})^0$ from phenylaminothioether moiety

**Table S19** TD-DFT-calculated electronic transitions of  $[1^{\text{Ox2}}]^{2+}$ , using B3LYP

Excitation energy (eV)	$\lambda$ (nm)	$f$	Transition	Assignment
1.1149	1112	0.0265	H[~62%L] → L[~95%L] (95%)	Intra-ligand CT in $(\text{L}^{\text{IBQ}})^0$ along with MLCT involving Ru → $(\text{L}^{\text{IBQ}})^0$
1.5706	789	0.038	H-1[~68%L] → L[~95%L] (10%)	Intra-ligand CT in $(\text{L}^{\text{IBQ}})^0$ along with MLCT involving Ru → $(\text{L}^{\text{IBQ}})^0$
			H[~62%L] → L+1[~76%L] (76%)	Combination of intra-ligand CT in $(\text{L}^{\text{IBQ}})^0$ and MLCT involving Ru → $(\text{L}^{\text{IBQ}})^0$
1.7779	697	0.053	H-4[~70%L] → L[~95%L] (12%)	Intra-ligand CT towards $(\text{L}^{\text{IBQ}})^0$ ring from appended phenyl ring of thioether moiety, along with MLCT involving Ru → $(\text{L}^{\text{IBQ}})^0$
			H-3[~79%L] → L[~95%L] (48%)	Intra-ligand CT from amino thioether moiety to $(\text{L}^{\text{IBQ}})^0$ along with MLCT involving Ru → $(\text{L}^{\text{IBQ}})^0$
2.0601	601	0.087	H-1[~68%L] → L[~95%L] (25%)	Intra-ligand CT in $(\text{L}^{\text{IBQ}})^0$ along with MLCT involving Ru → $(\text{L}^{\text{IBQ}})^0$
			H-7[~72%L] → L[~95%L] (70%)	Combination of intra-ligand CT within $(\text{L}^{\text{IBQ}})^0$ and MLCT involving Ru → $(\text{L}^{\text{IBQ}})^0$
2.2010	563	0.138	H-5[~94%L] → L [~95%L] (19%)	Combination of inter- and intra-ligand CT towards $(\text{L}^{\text{IBQ}})^0$ ring from appended phenyl ring of thioether moiety
			H-8[~52%M] → L[~95%L] (79%)	MLCT involving Ru → $(\text{L}^{\text{IBQ}})^0$ and intra-ligand CT in $(\text{L}^{\text{IBQ}})^0$

2.3038	538	0.069	H-4[~70%L] → L+1[~76%L] (15%)  H-3[~79%L] → L+1[~76%L] (35%)  H-1[~68%L] → L+1[~76%L] (31%)	Intra-ligand CT towards $(L^{IBQ})^0$ from appended phenyl ring of thioether moiety  Intra-ligand CT in $(L^{IBQ})^0$  Intra-ligand CT in $(L^{IBQ})^0$ and MLCT involving Ru → $(L^{IBQ})^0$
2.6563	466	0.112	H-11[~91%L] → L[~95%L] (28%)  H-9[~96%L] → L[~95%L] (21%)  H-7[~72%L] → L+1[~76%L] (38%)	Intra-ligand CT from amino thioether to $(L^{IBQ})^0$  Intra-ligand CT in $(L^{IBQ})^0$  Intra-ligand CT in $(L^{IBQ})^0$ and MLCT involving Ru → $(L^{IBQ})^0$
2.7292	454	0.0388	H-12[~83%L] → L[~95%L] (71%)	Intra-ligand CT in $(L^{IBQ})^0$
2.7671	448	0.087	H-8[~52%M] → L+1[~76%L] (47%)  H-7[~72%L] → L+1[~76%L] (27%)  H-11[~91%L] → L[~95%L] (9%)	MLCT involving Ru → $(L^{IBQ})^0$ and intra-ligand CT in $(L^{IBQ})^0$  Intra-ligand CT in $(L^{IBQ})^0$ and MLCT involving Ru → $(L^{IBQ})^0$  Intra-ligand CT from amino thioether to $(L^{IBQ})^0$
3.2867	374	0.0827	H-12[~82%L] → L+1[~76%L] (75%)	Intra-ligand CT from amino thioether to $(L^{IBQ})^0$